

## Sea-Ice Drift on the Northeastern Shelf of Sakhalin Island

GEORGY V. SHEVCHENKO

*Institute of Marine Geology and Geophysics, Far Eastern Branch, Russian Academy of Sciences, Yuzhno-Sakhalinsk, Russia*

ALEXANDER B. RABINOVICH

*Institute of Ocean Sciences, Department of Fisheries and Oceans, Sidney, British Columbia, Canada, and P. P. Shirshov Institute of Oceanology, Russian Academy of Sciences, Moscow, Russia*

RICHARD E. THOMSON

*Institute of Ocean Sciences, Department of Fisheries and Oceans, Sidney, British Columbia, Canada*

(Manuscript received 18 September 2002, in final form 2 April 2004)

### ABSTRACT

Ice-drift velocity records from coastal radar stations, combined with data from moored current meters and coastal wind stations, are used to examine sea-ice motion off the northeastern coast of Sakhalin Island in the Sea of Okhotsk. Ice motion is shown to be governed primarily by diurnal tidal currents and wind-induced drift, which explain 92%–95% of the total ice-drift variance. Diurnal tidal motions predominate off the northern Sakhalin coast, accounting for 65%–80% of the variance, while low-frequency wind-induced motions prevail off the south-central coast, accounting for over 91% of the ice-drift variance. Maximum diurnal tidal ice-drift velocities range from 90–110 cm s<sup>-1</sup> on the north coast to 10–15 cm s<sup>-1</sup> on the south coast, in good agreement with the barotropic model of Kowalik and Polyakov. The presence of diurnal shelf waves accounts for the strong diurnal currents on the steeply sloping northern Sakhalin shelf, while the absence of such waves explains the weak diurnal currents on the more gently sloping south-central shelf. Using a vector regression model, the authors show that wind-induced ice-drift “response ellipses” (the current velocity response to a unity wind-velocity forcing) are consistent with a predominantly alongshore response to the wind, with wind-induced currents most pronounced off the south-central coast where water depths are relatively shallow. Time–frequency analysis of wind and ice-drift series reveals that, in winter, when sea ice is most extensive and internally cohesive, the ice response is almost entirely aligned with the alongshore component of the wind; in spring, when sea ice is broken and patchy, the ice responds to both the cross- and alongshore components of the wind.

### 1. Introduction

Variations in ice distribution and concentration are of considerable practical significance for polar regions (Thorndike 1986; Wadhams 2000). Sea ice is one of the major factors affecting the winter operation of drill platforms and other coastal installations in the active oil and gas exploration of the northeastern shelf of Sakhalin Island in the Sea of Okhotsk (Fig. 1). Severe ice conditions are typical of the northeastern shelf of Sakhalin Island, with sea-ice fields in the region (Fig. 2) considered to be large, heavy, and fast moving. The ice-covered period lasts for over 6 months (November–May) (Preller and Hogan 1998; Martin et al. 1998) so that insight into ice dynamics and kinematics at this time of

year is important from both scientific and engineering perspectives.

Ice-field movement in the Sea of Okhotsk is forced primarily by the tides, surface currents, and winter winds (Martin et al. 1998). The ice response to wind and currents also strongly depends on the ice rheology and concentration (Hibler 1986; Wadhams 2000; Heil and Hibler 2002). The ice cover, in turn, affects the tidal motions and wind-driven currents. The presence of the coast produces additional effects, such as formation of land-fast ice and coastal friction, that cause further complications in the ice–ocean response (Overland and Pease 1988). In effect, the observed ice-drift motions result from a complex interacting system involving air, sea, ice, and land. Ice motions on the northeastern shelf of Sakhalin Island arise from two major factors: 1) strong diurnal tidal currents with speeds of 0.7–1.2 m s<sup>-1</sup> associated with shelf waves (Rabinovich and Zhukov 1984; Kowalik and Polyakov 1998) and 2) wind-driven currents with intermittent speeds up to 1 m s<sup>-1</sup>

---

*Corresponding author address:* Richard E. Thomson, Institute of Ocean Sciences, 9860 West Saanich Road, Sidney, BC V8L 4B2, Canada.  
E-mail: thomsonr@pac.dfo-mpo.gc.ca

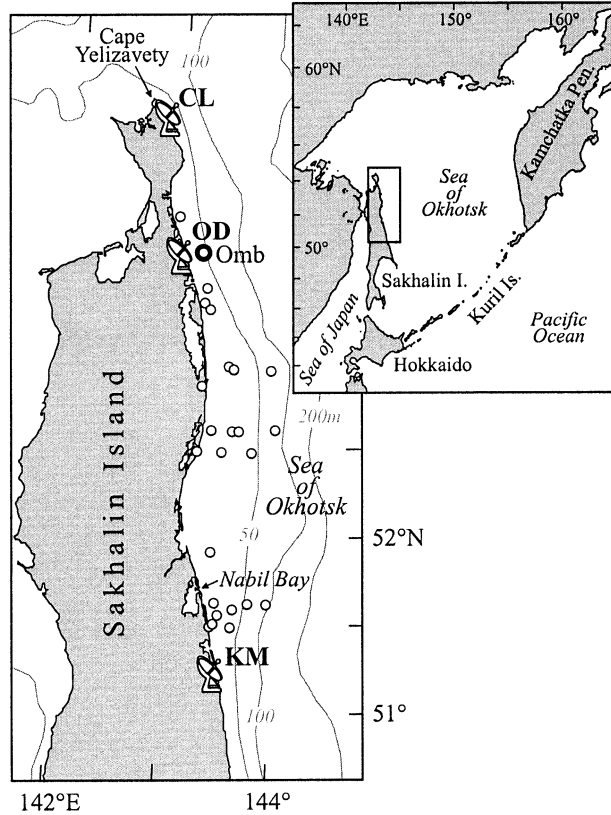


FIG. 1. Locations of coastal radar stations at Cape Levensterna (CL), Odoptu (OD), and Komviro (KM) used for monitoring of ice motions off the northeastern coast of Sakhalin Island. The current-meter station Ombinskaya (Omb) is indicated by a large circle; all other current meters are denoted by small circles.

generated by strong atmospheric events (Tambovsky et al. 2001).

The purpose of this paper is to use the multiyear, high-quality ice-drift data collected from three radar stations on the northeastern shelf of Sakhalin Island (Pokrasenko et al. 1987; Tambovsky et al. 2001) to examine sea-ice motion on the shelf. We also make use of the extensive summer current-meter data collected in the 1980s and 1990s on the northeastern shelf of Sakhalin Island (cf. Popudribko et al. 1998; Putov and Shevchenko 1998). Comparative analysis of ice-drift and ice-free summer currents allows us to examine seasonal changes in near-shore circulation and to determine how well shelf currents represent ice motion. We also compare summer versus winter tidal and wind-induced motions in the region to determine their seasonal variation. The ice-drift kinematics are found to be good indicators of dynamical processes in the region. Although ice concentration is expected to be a major factor affecting ice motion on Sakhalin shelf, we have not attempted in this study to examine the properties of the sea ice itself. For a thorough understanding on how internal ice stresses and ice deformation may affect ice drift, the reader is directed to the comprehensive literature on the subject (cf. Mellor 1986; Hibler 1986; McPhee 1986, 2002; Thorndike 1986; Geiger et al. 1998; Wadhams 2000; Heil and Hibler 2002; McNutt and Overland 2003).

## 2. Observations and data analysis

Coastal radar stations provide one of the most effective means for monitoring the sea-ice drift (Wakatsuchi and Ohshima 1990). The main impetus for radar ice tracking on the Sakhalin shelf from 1985 to 1995 was to obtain vector time series of ice-drift motion, similar

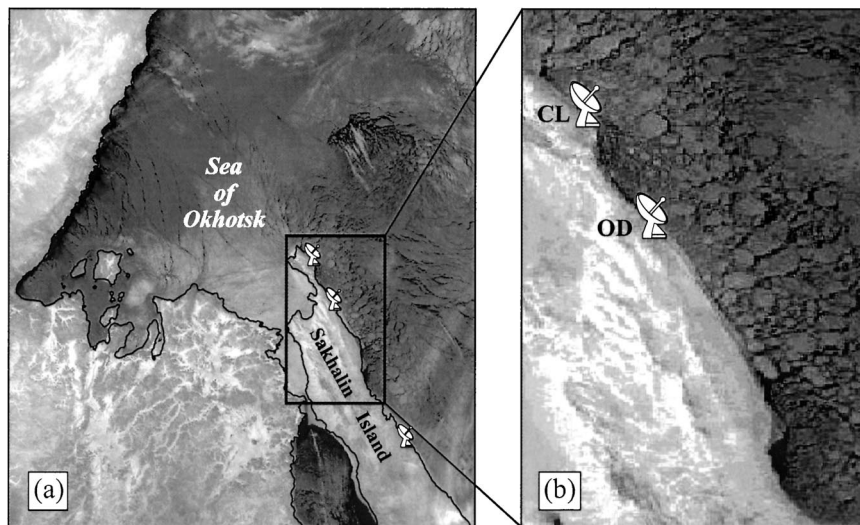


FIG. 2. National Oceanic and Atmospheric Administration Satellite NOAA-12 image of sea ice in the western Sea of Okhotsk on 8 Mar 2000. Radar station locations are superimposed on the image.

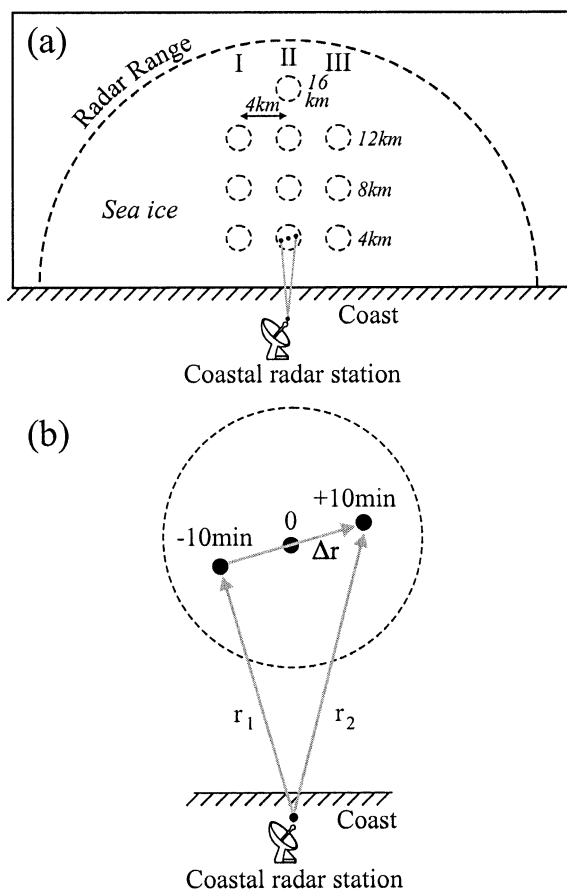


FIG. 3. A schematic of the CRS sea-ice measurement strategy. (a) Radar observation lines (I, II, and III) and locations of 1-km circular observational areas at selected offshore ranges of 4–16 km; (b) sea-ice position vectors needed to calculate ice drift within a selected circular area.

to those obtained for surface winds and currents (Pokrasenko et al. 1987). A radar antenna that is 50–60 m high provides accurate positioning of ice to a range of 15–20 km. Ice drift is estimated from the relative displacements of specific ice features within observational areas extending seaward along sampling lines running perpendicular to the coast (Fig. 3). Seaward-looking coastal radar stations (CRSs) were maintained at Cape

Levensterna (CL), Odoptu (OD), and Komrvo (KM) (Table 1; Fig. 1). The three sampling lines were 4 km apart and permitted ice-drift measurements within 1-km circular areas at selected distances from shore along three parallel lines from each radar station. Sampling circle locations along each of the lines were fixed at 4, 8, and 12 km seaward of the coast. The central line at CRS Odoptu had an additional circular area centered 16 km offshore (Fig. 3). The water depth for the sampling circles closest to shore (4 km seaward) was 10–15 m, while that for the most distant areas of coverage was ~50 m. Hourly ice-drift vectors were determined for major radar reflecting features on the ice floes within radar coverage circles. The positions were fixed three times per hour (at 10 min before, at, and 10 min after the hour). The ranges to the targets and respective azimuths (radial vectors from the radar antenna location) were defined for all 9 (10 for site OD) coverage circles. Data were then interpolated and averaged into hourly time series of eastward (cross-shore,  $u$ ) and northward (alongshore,  $v$ ) components of velocity. Local winds were measured simultaneously at hourly intervals at 10-m elevation.

Formation of coastal polynyas, which are common in this region (Alfultis and Martin 1987; Martin et al. 1998), leads to gappy radar sea-ice measurements. The year 1993 had the most extensive ice cover (Preller and Hogan 1998) and, therefore, the most continuous ice-drift time series. For the period 1 March to 8 June, 1993, we have a 100-day series at CL, a 73-day series at OD, and an 85-day series at KM. The quality of the observed data is high, with correlation of more than 0.9 between independent measurements of ice drift from various radar coverage circles at the same site. In addition, there is near-perfect consistency of tidal constants for data from different circles. Here, we use the data only from the central lines at each location, identifying different offshore circles as S1 (4 km), S2 (8 km), S3 (12 km), and S4 (16 km).

Figure 4 shows the simultaneous alongshore and cross-shore ice-drift motion recorded at the three radar stations in 1993 at the most remote offshore distances: 12 km (CL and KM) and 16 km (OD). The alongshore components of velocity are strong (60–80  $\text{cm s}^{-1}$ ) as

TABLE 1. Location of the CRSs on the Okhotsk Sea coast of Sakhalin Island and moored current-meter station on the northeastern Sakhalin shelf.

Station name	Position	Observational period	Offshore distance (km)	Sampling interval (min)
Cape Levensterna (CL)	54°14'N, 142°56'E	1992–95 <sup>a</sup>	4, 8, 12	60
Odoptu (OD)	53°26'N, 143°07'E	1985–96 <sup>a</sup>	4, 8, 12, (16) <sup>b</sup>	60
Komrvo (KM)	51°07'N, 143°34'E	1989–93 <sup>a</sup>	4, 8, 12	60
Ombinskaya (Omb) (current meter)	53°28'N, 143°17'E	1988 (31 Aug–16 Sep)	(15/45) <sup>c</sup>	15

<sup>a</sup> Only during ice-covered period.

<sup>b</sup> Only for the central sampling line.

<sup>c</sup> Current-meter depth/water depth (m).

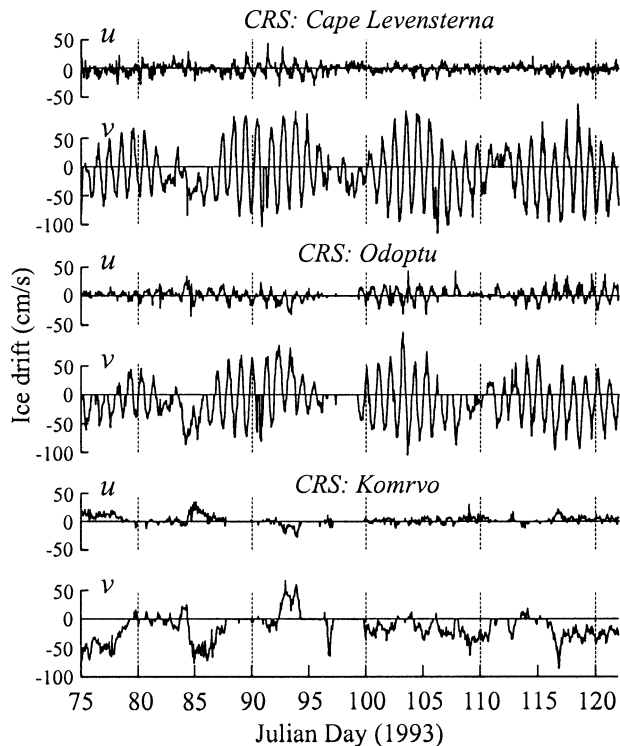


FIG. 4. Selected time series of ice drift on the northeastern shelf of Sakhalin Island, showing simultaneous records of 1993 ice-drift motions obtained from CRSs CL, OD, and KM.

compared with the cross-shore components ( $10\text{--}30\text{ cm s}^{-1}$ ) for all stations. Diurnal tidal currents with marked fortnightly modulation are ubiquitous features of the alongshore ice motion recorded by the northern and central radar stations, CL and OD (Fig. 4), but are nearly absent for the southern station, KM.

The radar measurements have been augmented with current-meter data collected from 1982 to 1998 on the northeastern shelf of Sakhalin Island (Popudribko et al. 1998; Putov and Shevchenko 1998). Station Ombinskaya (Omb) deployed in the end of August 1988 (Table 1) approximately 12 km offshore was especially useful because it was located only 4 km northward from CRS Odoptu (Fig. 1). The current-meter measurements reveal that alongshore currents are much stronger than cross-shore currents and that diurnal oscillations are the predominant form of variability.

#### a. Cross-shore variation in ice drift

Cross-correlation of ice-drift records for different offshore distances indicates that 1) in the cross-shore direction, alongshore drift is highly correlated ( $r^2 \sim 0.96\text{--}0.97$ ), slightly better than cross-shore drift ( $r^2 \sim 0.82\text{--}0.86$ ), and 2) ice-drift velocity is maximum at the most remote radar distance (16 km offshore) and gradually decreases with proximity to the coast. For alongshore motions, drift speeds decrease relative to the most off-

shore (16 km) site by 1% at 12 km, 3% at 8 km, and 8% at 4 km; for cross-shore motions, corresponding decreases are 13%, 18%, and 23%, respectively.

According to cross-spectral analysis (not shown for sake of brevity), alongshore ice-drift motions have high cross-shore coherence, steady near-zero cross-shore phase difference, and unity admittance for frequencies as high as 2.0–3.0 cycles per day (cpd) (i.e., for periods as short as 8–12 h). The energetic alongshore ice drift associated with diurnal and wind-driven currents (with frequencies less than 0.25–0.30 cpd) is nearly uniform across the shelf. Cross-shore drift currents also exhibit high cross-shore coherence and zero phase lag for frequencies as high as 1.2 cpd (periods as short as 20 h), but even at these frequencies, admittances become smaller with proximity to the coast. Admittance also decreases with decreasing frequency, indicating stronger boundary effects for long-period motions.

#### b. Time scales of ice-drift variability

We used spectral analysis to estimate the relative importance of various frequency components of ice-drift motions on the Sakhalin shelf. To improve the spectral estimates and increase the number of degrees of freedom  $\nu$ , the time series records were divided into 1024-h overlapping segments, and each segment was weighted using a Kaiser–Bessel window prior to application of the Fourier transform (Emery and Thomson 2003). The results of the separate analysis of the cross-shore ( $u$ ) and alongshore ( $v$ ) components for the 1993 ice-drift data are presented in Fig. 5. The main findings are as follows:

- 1) The alongshore (north–south) component of drift dominates at all frequencies, especially at tidal and subtidal frequencies.
- 2) There are strong spectral peaks at the northern stations CL and OD due to diurnal ( $K_1$ ,  $O_1$ ) tidal motions, whereas at southern station KM, the diurnal peak is weak.
- 3) Semidiurnal ( $M_2$ ) sea-ice oscillations are negligible at all sites. The only  $M_2$  peak is observed in the alongshore motions at radar station KM (Fig. 5).
- 4) In contrast to other high-frequency ice-drift observations (cf. Thorndike 1986; Padman and Kottmeier 2000; Heil and Hibler 2002), no inertial oscillations were found in the observed spectra of ice drift at radar stations CL, OD, and KM. Apparently, rotary inertial oscillations of ice in these areas (periods of about 15 h) are suppressed by the coastal boundary.
- 5) Spectra in the subtidal (low frequency) band are dominated by motions at approximately 5- and 12-day periods at all three radar stations. Spectra also suggest the existence of 21-day oscillations on the shelf. This latter peak is absent in Fig. 3 because of insufficient spectral resolution, but can be identified in higher-resolution spectra. The 5-, 12-, and 21-day

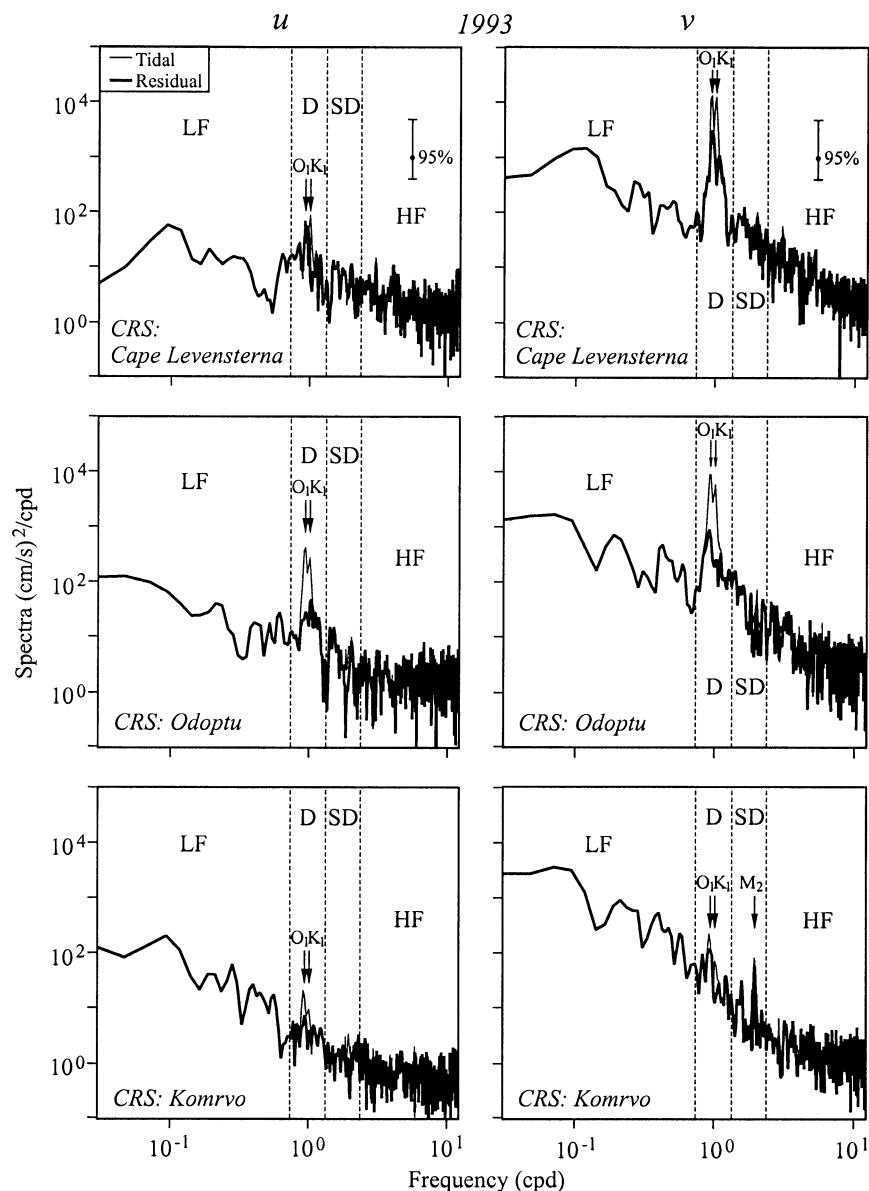


FIG. 5. Spectra of the original (thin line) and residual (detided) (thick line) cross-shore ( $u$ ) and alongshore ( $v$ ) ice-drift components measured from coastal radar stations at CRSs CL, OD, and KM (spectral resolution  $\Delta\omega = 0.0234$  cpd).

ice-drift oscillations also are present in local wind spectra (not shown), suggesting that the shelf motions are atmospherically induced.

Current-meter time series have durations of only 3–5 weeks and so cannot be used to examine low-frequency oscillations. The spectral frequency resolution also is much less than for the longer-duration ice-drift series. However, the general features of these spectra are the same in that alongshore currents prevail at all frequencies, diurnal tidal motions are dominant, subtidal motions are significant, and semidiurnal tidal peaks are negligible.

Guided by the peaks and gaps in the ice-drift spectra,

we partitioned the total velocity variance ( $\sigma_0^2$ ) into four frequency bands ( $f$ ) (Table 2): low frequency (LF),  $f < 0.8$  cpd; diurnal (D),  $f \approx 0.8$ – $1.4$  cpd; semidiurnal (SD),  $f \approx 1.5$ – $2.3$  cpd; and high frequency (HF),  $f > 2.3$  cpd. Here,

$$\begin{aligned} \sigma_n^2(\Delta f) &= \sigma_{nu}^2(\Delta f) + \sigma_{nv}^2(\Delta f) \\ &= \int_{\Delta f} [S(f, u) + S(f, v)] df \quad (1) \end{aligned}$$

is the total variance of ice-drift motion for a given coastal radar or current-meter station ( $n$ ) for a specified frequency band  $\Delta f$ . According to our variance parti-

TABLE 2. Variances in ice-drift and moored current-meter velocities for the northeastern shelf of Sakhalin Island for the four major frequency bands. Values in parentheses apply to the residual ice drift and currents obtained by subtracting the predicted tides. The far-right-hand column presents relative variances of the cross-shore ( $u$ ) and alongshore ( $v$ ) components of velocity.

Station year	Frequency band									
	Low frequency (LF)		Diurnal (D)		Semidiurnal (SD)		High frequency (HF)		All bands	
	( $\text{cm s}^{-1}$ ) <sup>2</sup>	(%)	( $\text{cm s}^{-1}$ ) <sup>2</sup>	$u/v$ (%)						
	Ice drift									
CL	325	14.8	1685	77.1	83	3.8	93	4.3	2185	4.0/96.0
1993	(325)	(35.1)	(431)	(46.6)	(79)	(8.5)	(90)	(9.7)	(925)	(8.1/91.9)
OD	412	25.5	1073	66.4	47	2.9	84	5.2	1616	5.8/94.2
1993	(412)	(52.8)	(243)	(31.2)	(44)	(5.7)	(80)	(10.3)	(780)	(8.2/91.8)
KM	844	91.5	31	3.4	19	2.0	28	3.1	923	5.9/94.1
1993	(844)	(92.5)	(24)	(2.6)	(16)	(1.8)	(27)	(3.0)	(912)	(5.8/94.2)
OD	464	21.1	1609	73.1	61	2.8	69	3.1	2202	7.8/92.2
1994	(464)	(52.8)	(101)	(31.2)	(56)	(5.7)	(64)	(10.3)	(685)	(19.8/80.2)
	Current meter									
Omb	80	3.3	2242	92.1	58	2.4	54	2.2	2434	20.7/79.3
1988	(80)	(48.3)	(6)	(3.6)	(24)	(14.8)	(53)	(33.2)	(163)	(55.1/44.9)

tioning, diurnal ice motion in 1993 at the north-central stations CL and OD accounted for 66%–77% of total variance and had 20–25 times the energy of diurnal motion at the southern station KM, and it was correspondingly stronger than the semidiurnal ice-drift motion at all stations. Low-frequency ice-drift motion accounted for 15%–25% of the total variance, except at site KM where it accounted for more than 91% of the variance. Semidiurnal and high-frequency ice motions together accounted for only 5%–8% of the total variance at all sites. Approximately 92%–94% of total variance was associated with alongshore motion (last column of Table 2).

The variance partitioning for the summer current-meter velocities at station Ombinskaya is similar to that for the ice-drift data, except that diurnal tidal currents are even more pronounced (accounting for 92% of the total energy), while low-frequency (subtidal) currents account for only 3%. Semidiurnal currents remain negligible (2.4%). In contrast to cross-shore ice-drift motion, cross-shore currents are relatively strong and account for almost 21% of the total variance (as compared with only 6%–8% for cross-shore ice-drift motion).

### c. Effects of ice concentration on ice drift

Comparison of the 1993 ice drift at CRS Odoptu with the 1988 currents for nearby station Omb indicates that the current variance ( $2434 \text{ cm}^2 \text{ s}^{-2}$ ) is about 1.5 times the ice-drift variance ( $1616 \text{ cm}^2 \text{ s}^{-2}$ ). This difference is mainly due to differences in diurnal motions (variances of 2242 and  $1073 \text{ cm}^2 \text{ s}^{-2}$ , respectively), which may be related to the prominent 18.6-yr nodal cycle in the diurnal tides. An analysis for extreme historical tides reveals that maximum diurnal tides on the northeastern shelf of Sakhalin Island occurred in 1968–69, 1987–88, and will occur every 18.6 yr thereafter.

During 1993, diurnal tides were approximately 20% weaker than in 1988, and so the diurnal variance in 1988 was presumably 1.45 times that in 1993. However, this still does not explain the factor of 2.1 difference in ice-drift variance between the two years. We therefore conclude that the difference is related to physical differences between the actual tidal currents and the ice-drift response to these currents arising from the anomalously high ice concentration observed in the Sea of Okhotsk in 1993 (cf. Preller and Hogan 1998). Both observations and numerical models indicate that internal ice stresses associated with high ice concentrations can significantly dampen tidal motions (Fissel and Tang 1991; Geiger et al. 1998; Heil and Hibler 2002).

We have compared the 1993 and 1994 ice-drift data at CRS Odoptu to characterize the importance of ice concentrations on ice drift. The 1994 concentrations on the northeastern shelf of Sakhalin Island were low as compared with 1993 (50%–70% and 80%–90%, respectively) (Preller and Hogan 1998). Accordingly, the 1994 ice-drift variance was about 1.5 times the 1993 variance, and this difference was associated with the much stronger diurnal ice drift in 1994 (Table 2). The ratio between the diurnal current variance at site Omb in 1988 ( $2242 \text{ cm}^2 \text{ s}^{-2}$ ) and the diurnal ice-drift variance at site OD in 1994 ( $1609 \text{ cm}^2 \text{ s}^{-2}$ ) is about 1.4, which is very close to the theoretical ratio for 1988–1994 for diurnal tides modified by the 18.6-yr nodal cycle. We therefore conclude that tidal ice drift in 1994 was relatively free, while that in 1993 was damped by high ice concentrations.

Because both the ice-drift and current-meter records indicate that over 92% of the total energy is in diurnal and low-frequency bands, the remaining analysis will focus on these two types of motions. Dominance of these two forms of ice motion is apparently typical for high

TABLE 3. Tidal ellipse parameters for the  $O_1$ ,  $K_1$ , and  $M_2$  tidal constituents for ice motions and currents on the northeastern shelf of Sakhalin Island. The Greenwich phase of the major axis has units of  $^\circ\text{G}$ , and the orientation of the major axis is in degrees true ( $^\circ\text{T}$ ). The sense of rotation is “-” for clockwise and “+” for counterclockwise.

Station year	Tidal constituent											
	$O_1$				$K_1$				$M_2$			
	Axis ( $\text{cm s}^{-1}$ )		Phase orientation		Axis ( $\text{cm s}^{-1}$ )		Phase orientation		Axis ( $\text{cm s}^{-1}$ )		Phase orientation	
Major	Minor	( $^\circ\text{G}$ )	( $^\circ\text{T}$ )	Major	Minor	( $^\circ\text{G}$ )	( $^\circ\text{T}$ )	Major	Minor	( $^\circ\text{G}$ )	( $^\circ\text{T}$ )	
CL 1993	38.6	2.8	(-) 12	358	46.4	2.7	(-) 95	356	0.7	0.1	(+) 83	311
1994	38.7	3.7	(-) 47	360	52.2	3.7	(-) 80	360	4.3	0.2	(+) 41	20
OD 1993	31.5	1.8	(-) 99	349	34.4	2.0	(-) 160	351	0.5	0.2	(+) 167	42
1994	36.5	4.0	(-) 89	355	46.7	4.1	(-) 156	359	1.2	0.2	(+) 196	112
KM 1993	4.5	0.1	(-) 25	335	2.3	0.7	(-) 118	19	2.7	0.02	(-) 45	347
1994	4.4	0.3	(+) 61	338	2.6	1.8	(-) 122	41	2.5	0.2	(-) 83	342
Omb 1988	41.8	4.5	(-) 81	337	46.5	8.3	(-) 145	338	4.1	0.3	(-) 109	344

latitudes (cf. Padman et al. 1992; Padman and Kottmeier 2000).

### 3. Tidal ice drift

This section examines tidally induced ice drift based on data for 1993 (March–June) and 1994 (April–May). To compare these data with ocean currents, we have mainly relied on ice-drift measurements from the most remote offshore distances, which we presume are least affected by land-fast ice. We also have used current-meter data from station Omb, as well as tidal amplitudes and phases computed from other available current measurements on the northeastern shelf of Sakhalin Island.

#### a. Tidal observations and analysis

Our harmonic analyses of the ice-drift and current tidal motions are based on the least squares method, with subsequent calculation of current ellipse parameters from component amplitudes and phases (cf. Pugh 1987). The major diurnal ( $K_1$  and  $O_1$ ) and major semidiurnal ( $M_2$ ) constituents are presented in Table 3. Other semidiurnal harmonics, as well as the computed monthly (Mm), fortnightly (Mf and Msf), and high-frequency (e.g.,  $MK_3$ ,  $MO_3$ ,  $M_4$ ) tidal harmonics, are not significant. The residual ice-drift series (obtained by removing the estimated tides) were then further examined for wind-induced ice drift (see section 4). We used the residual spectral energies for diurnal and semidiurnal frequency bands (Fig. 5; Table 2) to estimate possible errors in tidal amplitudes ( $\varepsilon_H$ ) and phases ( $\varepsilon_G$ ) (Pugh 1987):

$$\varepsilon_H = \sqrt{\frac{\sigma_{\Delta\omega}^2}{T\Delta\omega}} \quad \text{and} \quad \varepsilon_G = \frac{1}{H} \sqrt{\frac{\sigma_{\Delta\omega}^2}{T\Delta\omega}} \quad (\text{in radians}), \quad (2)$$

where  $\sigma_{\Delta\omega}^2$  is the nontidal residual variance in the averaging frequency band  $\Delta\omega$ ,  $T$  is the length of the time series, and  $H$  is the amplitude of the tidal constituent (Pugh 1987). Estimated  $\varepsilon_H$  values for the  $K_1$  and  $O_1$  harmonics range from 2.7–3.0  $\text{cm s}^{-1}$  (CL and OD) to

0.8–0.9  $\text{cm s}^{-1}$  (KM and Omb), while for the  $M_2$  constituent, values range from 0.4  $\text{cm s}^{-1}$  (KM) to 1.2  $\text{cm s}^{-1}$  (Omb). The  $K_1$  and  $O_1$  phase errors ( $\varepsilon_G$ ) for the alongshore component ( $v$ ) were 1.2 $^\circ$  for Omb, 3.4 $^\circ$ –4.5 $^\circ$  for CL and OD, and 10 $^\circ$ –18 $^\circ$  for KM. For  $M_2$  the phase errors were 73 $^\circ$  (CL), 80 $^\circ$  (OD), 8.5 $^\circ$  (KM), and 17 $^\circ$  (Omb). Amplitudes of cross-shore ( $u$ ) motions are a factor of 15–20 times smaller than those of alongshore motions, and so the respective phase errors for the  $u$  components are 15–20 times those for the  $v$  components. Results from harmonic analysis of the ice records (Table 3) are consistent with numerical tidal models for the Sea of Okhotsk (Suzuki and Kanari 1986; Kowalik and Polyakov 1998; Nakamura et al. 2000), which produce strong diurnal currents near the northern end of Sakhalin Island (Cape Yelizavety) and weakening diurnal currents to the south (Fig. 6).

Ellipses of tidal ice drift for the major diurnal constituents,  $K_1$  and  $O_1$ , are similar for stations CL and OD (Table 3). Moreover, the ice-drift ellipses are in general agreement with the respective ellipses for tidal currents measured at nearby current-meter station Omb. In both datasets, ellipses are clockwise and their axes stretched along the Sakhalin coastline. The slight difference in ellipse orientation between ice drift and currents is apparently related to local changes in coastline orientation. Maximum  $K_1$  and  $O_1$  currents at the current-meter station Omb were about 40–50 and 35–40  $\text{cm s}^{-1}$ , respectively, similar to those for the 1994 ice-drift motions. Other measurements of tidal currents in this region (cf. Rabinovich and Zhukov 1984; Popudribko et al. 1998; Putov and Shevchenko 1998) agree closely with the 1994 ice-drift measurements and with the results of the numerical modeling by Kowalik and Polyakov (1998). However, the 1993 tidal diurnal ice-drift motions were approximately 30%–35% weaker than those observed in 1994 and those predicted numerically by Kowalik and Polyakov (1998; Tables 2 and 3; Fig. 6).

Spectra of the 1993 alongshore ( $v$ ) ice drift (Fig. 5) obtained after subtraction of estimated mean tidal ice drift show significant diurnal peaks in the residual ice

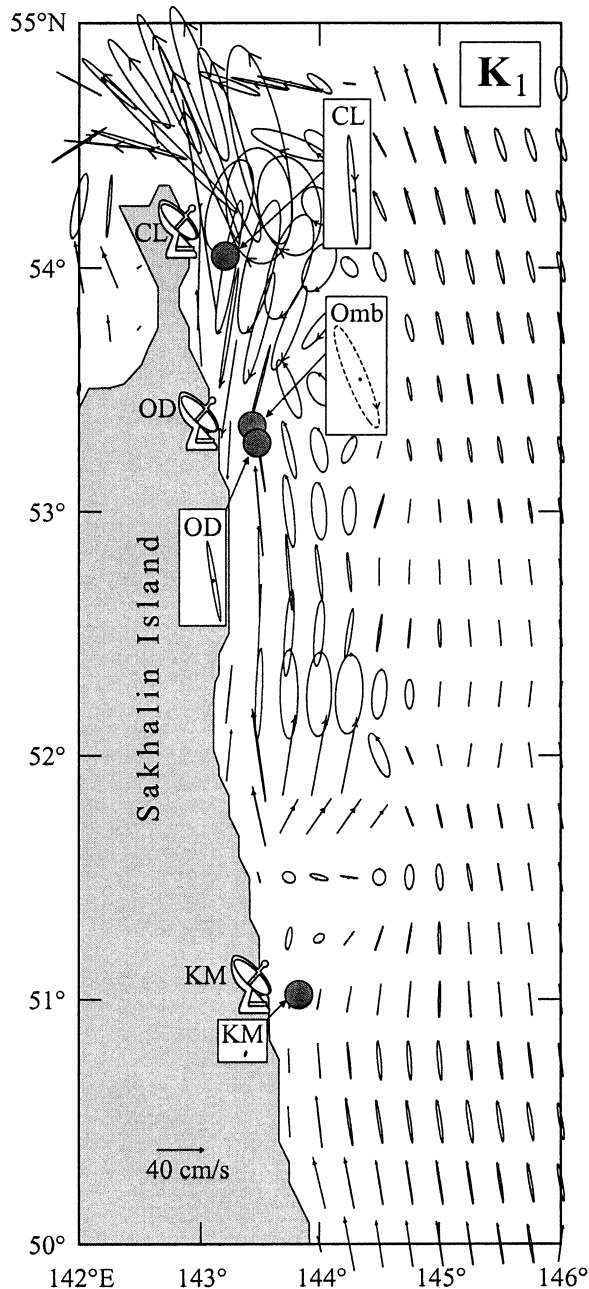


FIG. 6. Maps of computed currents for the  $K_1$  diurnal tidal constituent for the northeastern shelf of Sakhalin Island from numerical tidal simulations by Kowalik and Polyakov (1998) and observed  $K_1$  tidal ellipses recorded by CRSs CL, OD, and KM and by current-meter station Omb.

motion. Residual motions account for 25.6% of the total diurnal variance of  $1685 \text{ cm}^2 \text{ s}^{-2}$  at CL and for 22.6% of the total variance of  $1073 \text{ cm}^2 \text{ s}^{-2}$  at OD (Table 2). In contrast, the 1994 residual diurnal ice drift was considerably smaller: only 6.3% of  $1609 \text{ cm}^2 \text{ s}^{-2}$  at OD. For comparison, the residual diurnal currents at station Omb were negligible and account for only 0.3% of  $2242 \text{ cm}^2 \text{ s}^{-2}$ . Results indicate the regular deterministic char-

CRS: Odoptu (1993)

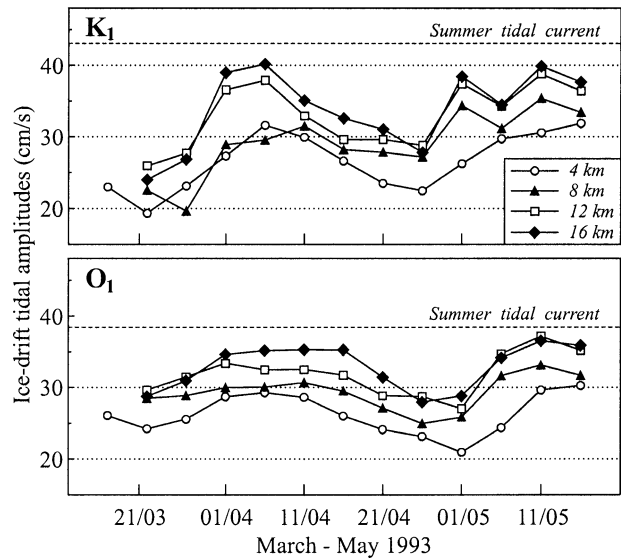


FIG. 7. Time variations of the alongshore  $K_1$  and  $O_1$  amplitudes for the period Mar–May 1993 recorded from CRS OD at 4, 8, 12, and 16 km offshore. Dashed line shows the current amplitudes recorded in summertime at the nearby station Omb.

acter of diurnal currents on the Sakhalin Island shelf during ice-free periods and the less regular, partly random behavior of diurnal ice-drift motions during ice-covered periods. These irregularities were less pronounced in 1994 when compared with 1993 because of the lower ice concentrations in 1994.

In the cross-shore direction, the  $K_1$  and  $O_1$  ellipses are quite similar (not shown for sake of brevity), suggestive of high-quality and reliable ice-drift data. Ellipses are flat and elongated along the coastline [e.g., at CRS Odoptu the azimuths of the major axes are between  $347.8^\circ$  (degrees true) and  $350.6^\circ$  for  $K_1$  and between  $346.4^\circ$  and  $348.6^\circ$  for  $O_1$ ] and all have clockwise rotation. Tidal ice-drift amplitudes at CRS Odoptu gradually increase seaward from  $28.4$  (at S1) to  $34.4 \text{ cm s}^{-1}$  (at S4) for  $K_1$  and from  $27.5$  to  $31.5 \text{ cm s}^{-1}$  for  $O_1$ . Presumably, this seaward increase in amplitude is due to reduced coastal and bottom friction, which, in turn, arise from the effects of land-fast ice and internal ice stress within an ice-drift boundary layer (cf. Thorndike and Colony 1982; Overland and Pease 1988). A typical width of land-fast ice in the study region is 2–3 km (cf. Tambovsky et al. 2001). The tidal ice-drift motions within the near-coastal boundary layer were found to have significant temporal variations. For example, at the 16-km distance (S4) at site OD, the  $K_1$  amplitudes varied with time from 24 to  $40 \text{ cm s}^{-1}$ , and the  $O_1$  amplitudes varied from 27 to  $38 \text{ cm s}^{-1}$ . These temporal variations are well correlated for different offshore distances and for different constituents (Fig. 7). Comparison of tidal amplitude distributions with 1993 satellite images of ice on the Sakhalin shelf (Martin et al. 1998; Preller and

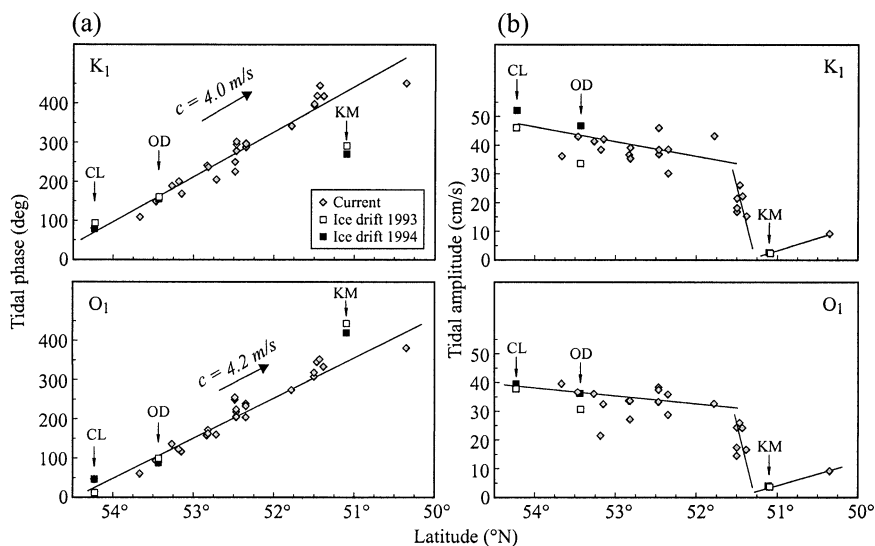


FIG. 8. Alongshore (from north to south) variations in the (top)  $K_1$  and (bottom)  $O_1$  tidal (a) phases and (b) amplitudes estimated from current-meter and ice-drift observations on the northeastern shelf of Sakhalin Island (both for 1993 and 1994). Error bars are computed but not seen because they do not exceed the size of the symbols. Solid lines in (a) are least squares estimates of mean phase speed  $c$  for the  $K_1$  and  $O_1$  tidal waves; arrows show the southward wave propagation. Solid lines in (b) are least squares estimates for tidal amplitudes.

Hogan 1998), as well as with the coastal visual observations made during the radar ice measurements (Tambovsky et al. 2001), indicates that minimum tidal ice-drift amplitudes (in particular, those in April 1993) occurred during periods of the highest ice concentrations (>85%–90%) in this region. Maximum tidal amplitudes were associated with periods of lowest ice concentrations (<50%–60%). This suggests that in May when the ice began to melt and the ice-covered area decreased the ice drift became free and tidal motions became as intensive as in summer (summer tidal amplitudes at station Omb are indicated in Fig. 7 by a dashed line).

#### b. Alongshore tidal variations

To examine the spatial variations in diurnal tidal motion along the Sakhalin coast, we combined the ice-drift data for 1993 and 1994 and the data from 32 current-meter moorings on the northeastern shelf of Sakhalin Island. The current measurements were made in different years and different seasons. Despite the different observation dates, the computed tidal constants are in good agreement, indicating the stable predominantly barotropic character of diurnal tides in this region. Plots of the alongshore current amplitudes and phases for the  $K_1$  and  $O_1$  constituents are presented in Fig. 8. Large errors for cross-shore phases and relative amplitudes, which are 15–20 times those for the alongshore component (see section 3a) prevent us from the constructing corresponding plots for the cross-shore motions. Figure 8 is consistent with the results in Fig. 6 and has the same specific features, namely,

- 1) a zone of large-amplitude  $K_1$  tidal currents bordering the northeastern end of Sakhalin Island,
- 2) an abrupt southward decrease in  $K_1$  tidal velocities beginning around  $51.5^\circ\text{N}$  latitude,
- 3) a zone of minimum currents at approximately  $51.0^\circ$ – $51.2^\circ\text{N}$  latitude, and
- 4) evidence (from the alongshore  $K_1$  phase change) for southward propagation of the  $K_1$  tidal wave along the coast of Sakhalin.

#### c. Modeling diurnal shelf waves

Rabinovich and Zhukov (1984) were the first to suggest that strong diurnal currents on the northeastern shelf of Sakhalin Island are produced by tidally generated, coastally trapped shelf waves. Because diurnal shelf waves are formed through the joint effect of earth's rotation and shelf topography rather than gravity, their energy is predominantly kinetic, so these waves produce negligible sea level variations but significant tidal currents (LeBlond and Mysak 1978; Mysak 1980). Southward propagation of diurnal tidal motions along the northeastern coast of Sakhalin Island is consistent with the theoretical direction of shelf waves (cf. Mysak 1980; Crawford and Thomson 1984). A least squares analysis using the observed phases of the diurnal currents gives wave phase speeds  $c = 4.0 \text{ m s}^{-1}$  for  $K_1$ , and  $c = 4.2 \text{ m s}^{-1}$  for  $O_1$  (Fig. 8a). Ice-drift phases at stations CL and OD are in good agreement with current-meter phases and phase speed estimates, while the KM phases are outliers. Slightly different phase speeds for the two di-

urnal constituents (which is evidence for wave dispersion) are in good agreement with theoretical estimates of phase speed of diurnal shelf waves for the central part of the northeastern Sakhalin shelf ( $3.9 \text{ m s}^{-1}$  for  $K_1$  and  $4.3 \text{ m s}^{-1}$  for  $O_1$ ) presented by Rabinovich and Zhukov (1984). Similar values were obtained by Kowalik and Polyakov (1998) based on their barotropic numerical model of the Okhotsk Sea tides, specifically,  $c = 3.35 \text{ m s}^{-1}$  ( $K_1$ ) and  $c = 3.70 \text{ m s}^{-1}$  ( $O_1$ ) for the central part of the northeastern shelf of Sakhalin Island.

Current amplitudes (Fig. 8b) have a complicated alongshore structure. On the northern part of the shelf (from  $54.4^\circ$  to  $51.8^\circ\text{N}$ ), amplitudes of alongshore diurnal currents remain strong, approximately  $35\text{--}50 \text{ cm s}^{-1}$  for  $K_1$  and  $30\text{--}40 \text{ cm s}^{-1}$  for  $O_1$ . However, in the vicinity of Nabil Bay ( $51.8^\circ\text{N}$ ), the  $K_1$  and  $O_1$  amplitudes drop abruptly, with diurnal currents in the region  $51.3^\circ\text{--}50.3^\circ\text{N}$  having speeds of only a few centimeters per second. The numerical simulations by Kowalik and Polyakov (1998) show a similar alongshore current structure with strong diurnal currents on the northern shelf attenuating rapidly southward, reaching minimum velocities in the vicinity of  $50.5^\circ\text{--}51.5^\circ\text{N}$  (Fig. 6). Using trajectory data from 20 surface Argos drifters in the Sea of Okhotsk (August–September 1999), Ohshima et al. (2002) also found strong diurnal tidal currents over the shelf shallower than 200 m north of  $51.5^\circ\text{N}$ , but weak diurnal currents south of  $51.5^\circ\text{N}$ . The area of broken ice in the satellite image presented in Fig. 2 also closely coincides with the zone of strong computed diurnal tidal currents (Fig. 6) located north of  $51.5^\circ\text{N}$ .

The model by Rabinovich and Zhukov (1984) accounts for the phase behavior of the currents (Fig. 8a) but not the amplitude variations (Fig. 8b). An alternate model, which was successfully applied by Foreman and Thomson (1997) to the Pacific shelf of Vancouver Island, involves frictional attenuation of diurnal shelf waves. According to this model, friction and scattering can cause the amplitudes of the alongshore diurnal currents  $v$  to decay exponentially, such that  $v(y) \sim \exp(-\delta y)$ , where  $y$  is the distance from the source area, and  $\delta$  is the decay coefficient. [Numerical results of Kowalik and Polyakov (1998) indicate that the source area of diurnal shelf waves on the northeastern shelf of Sakhalin Island is Cape Yelizavety, the northernmost end of the island.] However, for the Sakhalin coast the observed alongshore velocity changes are not accurately described by an exponential decay (see Fig. 8b). We, therefore, conclude that the southward amplitude decay arises not from friction and scattering but from alongshore changes in the cross-shore shelf topography, which are the key factors influencing shelf waves (cf. Mysak 1980; Crawford and Thomson 1984). The model by Rabinovich and Zhukov (1984) did not take these changes into account; all calculations were made for one cross-shelf profile ( $\sim 53^\circ\text{N}$ ). Consequently, for the present model, we undertook several numerical calculations to determine if current amplitude variations, in

particular the abrupt drop in current amplitudes in the central part of the northeastern Sakhalin shelf, could be due to the rapid change in topography along this part of the shelf (Fig. 9a).

The linearized, barotropic long-wave equations for alongshore propagating free waves of angular frequency  $\omega$  and wavenumber  $k$  in a rotating coordinate system yield the following equation for the cross-shore structure of the sea level displacement  $\zeta(x)$  (LeBlond and Mysak 1978):

$$\zeta''(x) + \frac{h'(x)}{h(x)}\zeta'(x) + \left[ \frac{\omega^2 - f^2}{gh(x)} - \frac{fk}{\omega} \frac{h'(x)}{h(x)} - k^2 \right] \zeta(x) = 0, \quad (3)$$

with boundary conditions

$$\zeta(x) \rightarrow 0 \quad \text{as } x \rightarrow \infty \quad \text{and} \quad (4a)$$

$$h[\omega\zeta'(x) + fk\zeta(x)] = 0 \quad \text{at } x = 0. \quad (4b)$$

Here,  $x$  and  $y$  are the offshore (eastward) and alongshore (northward) directions, respectively;  $h = h(x)$  is the depth (uniform alongshore); and  $' \equiv d/dx$ . For subinertial frequencies ( $\omega < f$ ), (3)–(4) describe two types of trapped coastal waves: gravity-dominated Kelvin waves and quasigeostrophic continental shelf waves (LeBlond and Mysak 1978). Kelvin waves generate large sea level oscillations with relatively weak shelf currents, whereas shelf waves generate strong shelf currents with small sea level oscillations (Mysak 1980; Yefimov and Rabinovich 1980). Shelf waves of diurnal period have been shown to be responsible for strong diurnal currents on the northeastern shelf of Sakhalin Island (Rabinovich and Zhukov 1984; Suzuki and Kanari 1986; Kowalik and Polyakov 1998; Nakamura et al. 2000).

Rabinovich and Zhukov (1984) solved (3) and (4) using the initial parameter method with a steplike approximation to the shelf depth profile. Here, we have used the Brink and Chapman (1987, hereinafter BC87) algorithms, which better approximate the depth profiles and shelf wave dispersion curves. We applied the BC87 algorithms for 15 different cross-shore depth profiles along the northwestern coast of Sakhalin Island (Fig. 9a). Although the numerical integration scheme assumes uniform alongshore topography, one can compute changes in the shelf wave structure and parameters along the island from dispersion curves for different profiles (cf. Crawford and Thomson 1984). Shelf waves exist only on the negative side of the dispersion diagrams (Fig. 9b), indicating that the waves propagate southward on the Okhotsk shelf of Sakhalin Island with the coast on their right.

Computed dispersion curves (Fig. 9) are similar for the entire coast. However, the maximum allowable frequency for first-mode waves differs significantly for the different depth profiles (lines 1–15). Similarly, the wavelengths/phase speeds of the  $K_1$  and  $O_1$  shelf waves

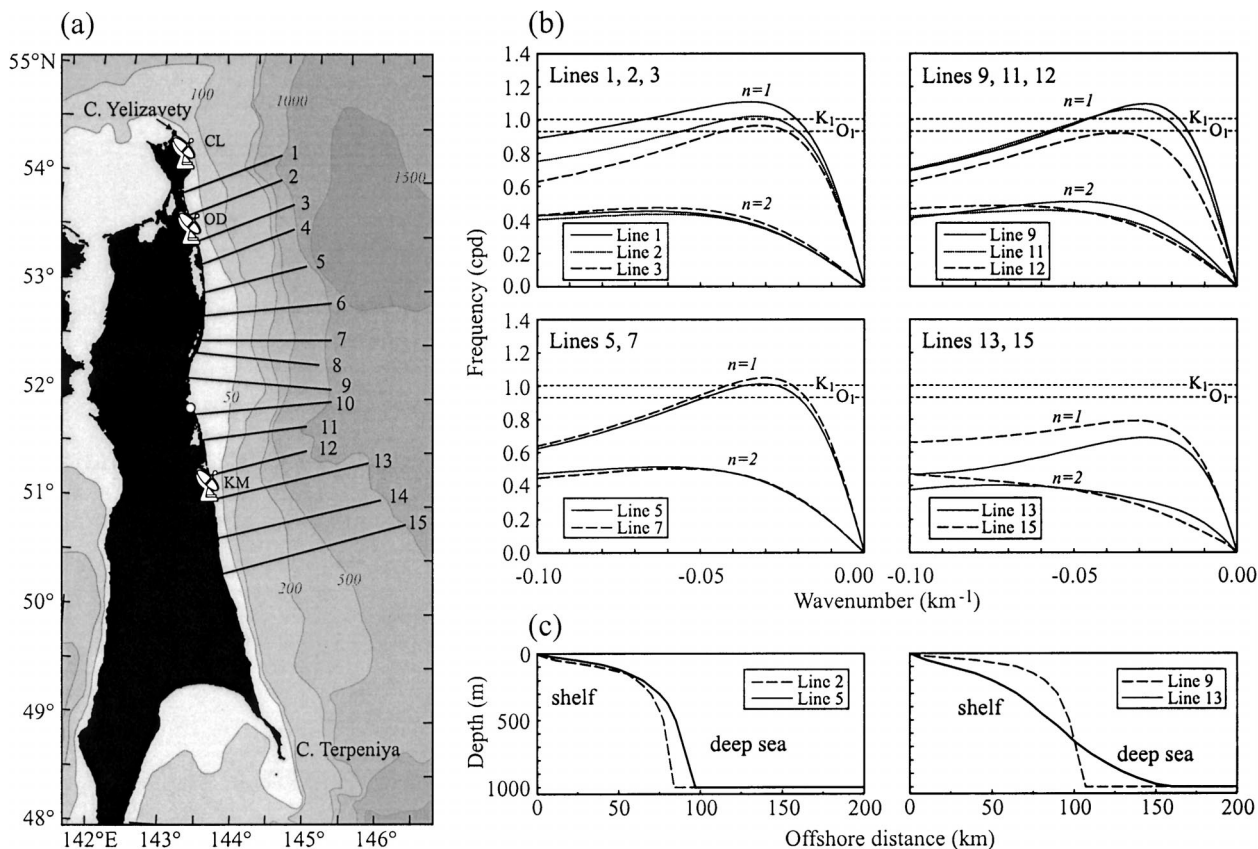


FIG. 9. (a) Bottom topography for the northeastern shelf of Sakhalin Island. Depth profiles along cross-shelf lines 1–15 are used for computation of shelf wave modes. Locations of CRSs CL, OD, and KM are indicated. (b) Dispersion curves for first- and second-mode barotropic shelf waves computed for the 1–15 cross-shelf depth profiles. (c) Cross-shelf depth profiles for lines 2, 5, 9, and 13. Dispersion curves in (b) for lines 4, 6, 8, 10, and 14 are not presented since they closely coincide with the corresponding curves for lines 2, 7, 9, 11, and 13, respectively.

differ along the coast. The wider shelf along the northernmost part (line 1) and the central part of the northeastern coast of the island (lines 8 and 9) support longer-wavelength, more rapidly propagating shelf waves, while the narrower shelf between these two areas (lines 2–5) supports shorter and slower shelf waves. Maximum first-mode shelf wave frequencies depend on the depth contrast between the coastal shelf and the open ocean. Frequencies are normally higher for well-defined shallow shelves and steep slopes and lower for smooth gentle shelves and slopes. For the area seaward of CRS Komviro (lines 13–15), computed dispersion curves for first-mode shelf waves are below the frequency threshold for diurnal tides (Fig. 9b). Presumably, it is for this reason that diurnal tidal currents are negligible in this region (Figs. 6 and 8b). Ohshima et al. (2002) came to a similar conclusion based on the shelf wave dispersion relations for the averaged bathymetry north and south of 51.5°N. According to these authors, first-mode diurnal shelf waves can only exist north of 51.5°N.

Figure 10 shows the alongshore variation in the maximum frequency of the first-mode shelf wave and the corresponding phase speeds of this mode for the  $K_1$  and

$O_1$  tidal frequencies. There is close agreement between the alongshore zone of permitted diurnal shelf waves (Fig. 10a) and the zone of significant diurnal currents (Fig. 8b). On the basis of these results, we identify three distinct regions of diurnal tidal current behavior along the northeastern shelf of Sakhalin Island (these regions are marked by straight lines in Fig. 8b):

- 1) 54.5° to 51.5°N: a region of strong diurnal currents, with gradual north-to-south decrease in amplitude,
- 2) 51.5° to 51.3°N: a region in which there is an abrupt drop in diurnal current amplitude, and
- 3) 51.3° to <50.5°N: a region of weak diurnal currents.

As indicated by Figs. 9b and 10a, the first region is a zone of strong diurnal shelf waves, the second is a transition zone composed of evanescent diurnal shelf waves (maximum frequency drops below the threshold frequency), and the third is a forbidden zone for diurnal shelf waves. Although we lack observational data south of 50.5°N and have not computed shelf wave modes for higher latitudes, the upturn of the southern end of the curve in Fig. 10a suggests a possible area for diurnal shelf waves, and associated strong diurnal currents,

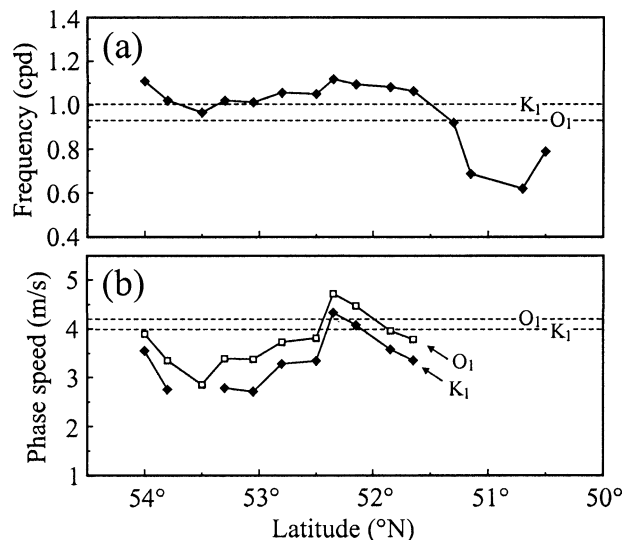


FIG. 10. Alongshore variations in computed values of (a) maximum frequency and (b) corresponding phase speeds for the first mode of shelf waves along the northeastern coast of Sakhalin Island. Dashed lines in (a) denote the  $K_1$  and  $O_1$  tidal frequencies; dashed lines in (b) denote the mean phase speeds (for  $K_1$  and  $O_1$  tides) estimated from the observations (cf. Fig. 8a).

south of our study region. Numerical computations of tidal currents for the Sakhalin shelf by Kowalik and Polyakov (1998) support this possibility (cf. Fig. 6).

Several details are worth noting. For example, both the numerical modeling of tides in the Sea of Okhotsk by Kowalik and Polyakov (1998) (Fig. 6) and our estimates of the observed  $K_1$  tidal currents (Fig. 8b) suggest a local minimum in  $K_1$  coastal currents around  $53.5^\circ\text{N}$ . According to the numerical calculations, the maximum frequency of the first-mode waves has a local minimum in this area (Fig. 10a), dropping below the threshold frequency for  $K_1$  waves but not for  $O_1$  waves. As a result,  $K_1$  currents become weaker but  $O_1$  currents remain about the same as currents to the north (Fig. 8b). As indicated by Fig. 10b, the predicted phase speeds of  $K_1$  and  $O_1$  shelf waves (about  $3.4$  and  $3.8$   $\text{m s}^{-1}$ , respectively) are slightly less than the observed speeds of  $4.0$  and  $4.2$   $\text{m s}^{-1}$  (Fig. 8a), consistent with the influence of stratification upon these waves (cf. Crawford and Thomson 1984). In all our computations, the second-mode shelf waves have frequencies far below diurnal tidal frequencies (Fig. 9b) and are not expected to contribute to diurnal tidal currents on the northeastern shelf of Sakhalin Island.

Several numerical experiments were undertaken to quantify the effect of bottom friction on propagating shelf waves using the simplifying assumption for the bottom boundary layer term

$$Y_B = (\rho_0 h)^{-1} \tau_B^y(x, y; t) \quad (5)$$

in BC87, where  $\rho_0$  is the mean density,  $t$  is time, and  $\tau_B^y$  is the bottom stress. The BC87 algorithms first calculate the frictionless case (3)–(4) and then introduce

the term (5) to iterate directly for the complex phase speeds  $\hat{c}_n$  of the free modes of the system. The imaginary part of  $\hat{c}_n$  describes the damping time of the corresponding mode. Because of high current velocities, the shelf waves decay much faster than gravity waves (e.g., the Kelvin wave), causing intensive dissipation of diurnal tidal energy over the shelf (cf. Rabinovich and Shevchenko 1984). Our computational estimates of the real part of  $\hat{c}_n$  indicate that friction reduces the phase speed, but for the diurnal frequencies, this effect is only a few percent. In summary, our tidal analysis confirms that diurnal shelf waves play a key role in ice-drift motions on the northeastern shelf of Sakhalin Island and that the main properties of shelf waves, which are well established analytically (cf. LeBlond and Mysak 1978; Mysak 1980), can be used to describe the principal features of tidal ice motions in this area.

#### d. Diurnal tidal currents and ice behavior

Satellite imagery suggests a possible linkage between ice concentration and tidal currents. As indicated by Fig. 2, the area of broken ice closely coincides with the zone of strong diurnal tidal currents associated with diurnal shelf waves (see Fig. 6). The relatively small wavelength scales ( $\sim 300$  km) of these waves means that diurnal tidal currents in the vicinity of CL and in the area southward of OD ( $\sim 150$  km separation) are roughly one-half of a wavelength apart and therefore flow in *opposite directions* at any given stage of a diurnal cycle (Fig. 11). Southward tidal drift at site CL corresponds to northward drift at the southern areas, and vice versa. During a rising tide, tidal currents in the northern and southern areas are directed toward one other (Fig. 11a), causing convergence of the sea ice. Twelve hours later, during a falling tide, current vectors are directed away from one other (Fig. 11b), causing divergence of the sea ice. This convergence–divergence action is focused at approximately  $53^\circ 15' \text{N}$  and appears to be a possible cause for the ice cracking and hummocking observed in Fig. 2. Almost the same area of broken ice on the northeastern shelf of Sakhalin Island is clearly visible in satellite images of 24 March 1979 and 5 April 1979 (Figs. 4b,c in Wakatsuchi and Martin 1990). Moreover, in the image of 24 February 1979 (Fig. 4a in Wakatsuchi and Martin 1990), this zone totally coincides with the zone of the “Sakhalin polynya” commonly observed in this zone (cf. Martin et al. 1998). So, we assume that intensive shelf-wave-induced tidal currents not only contribute to ice breaking but also maintain the ice opening and polynya formation.

The intensity of this process presumably depends on the speed of the tidal currents. Maximum diurnal tides and associated currents normally occur when the lunar declination is greatest (“tropical tides”), while minimum diurnal motions occur when the declination is close to zero (“equatorial tides”) (Fig. 12). Fortnightly modulation of diurnal tides has a period of 13.61 days

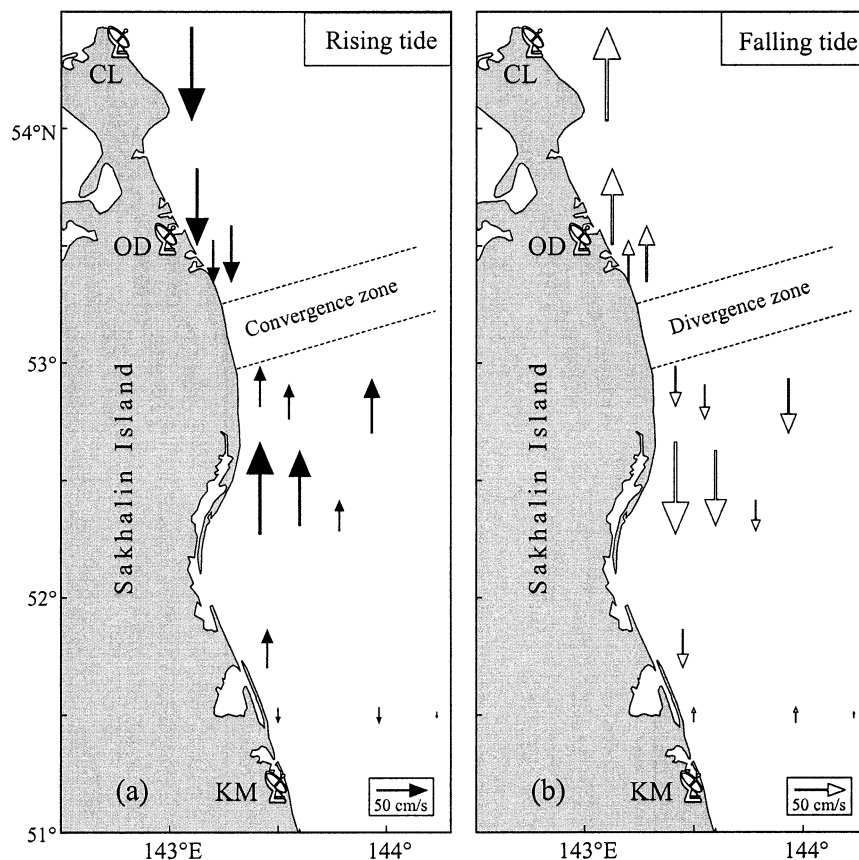


FIG. 11. Maximum (tropical) computed alongshore diurnal tidal currents on the northeastern shelf of Sakhalin Island during (a) a rising tide and (b) a falling tide based on current-meter and ice-drift measurements. (Measurements were obtained during different years and seasons. These measurements were then used to estimate the harmonic constants from which we computed tidal currents for the time of maximum lunar declination.)

( $\approx 1/2$  of the “nodical month”) (Pugh 1987). In terms of the tidal constituents, fortnightly nodical modulation is associated with the superposition of  $K_1$  and  $O_1$  diurnal harmonics: maximum diurnal tidal sea levels and currents occur when the  $K_1$  and  $O_1$  are in phase and minimum when they are out of phase. This fortnightly modulation of tidal currents affects wind-forced ice drift (see section 4) on the Sakhalin shelf. During the period of equatorial tidal currents, if air temperature is sufficiently low and winds are not too strong, the sea ice can freeze into an extensive cohesive mass that would not respond to the local wind. Such a situation occurred on 6–11 April 1993 at site OD; tidal currents at the time of a near-zero lunar declination were weak, air temperature was low, and the ice froze in place. As a result, the correlation coefficient between the alongshore wind and ice drift dropped to near zero (Fig. 12). This observation is in agreement with theoretical results of Hibler (1986) for an idealized one-dimensional system with and without plastic ice interaction (his Fig. 6). More specifically, for times of strong ice interaction, there is a threshold wind speed of about  $4.5 \text{ m s}^{-1}$  below which the ice does not move (unlike the case for free ice). However, once

this threshold wind speed is exceeded, the ice begins to move quickly and, for increasing wind speed, ice flow velocity begins to rapidly approach that for free ice.

We remark here that the ice did not stop moving during two other periods of equatorial tides (22–26 March and 19–22 April 1993) because of strong winds and high air temperatures, respectively. In general, strong tropical diurnal tidal currents are likely to contribute to ice breaking and formation of free ice, while weak equatorial tidal currents likely result in an increase in ice compactness. The resulting feedback interaction between tidal currents and ice could significantly affect both processes.

#### 4. Wind-induced ice drift

Low-frequency motions account for roughly 15% of the total variance of ice drift at radar station CL, 21%–25% at OD, and 91% at KM (Table 2). In part, the dominance of low-frequency motions at site KM is due to the negligible diurnal tidal energy at this station as compared with the two other stations (only 3.4% at KM

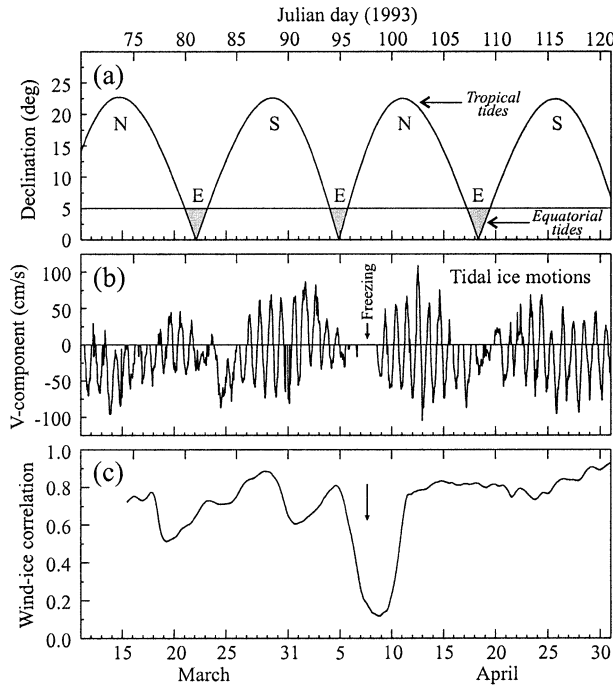


FIG. 12. Relationship between lunar tides and alongshore ice drift. (a) Lunar declination for Mar–Apr 1993; (b) alongshore ice drift at station OD; and (c) temporal variation in the correlation coefficient between the alongshore component of wind velocity and ice drift at CRS OD. Letters “N” and “S” indicate maximum north and south lunar declination; letter “E” marks near-zero (equatorial) declination. The arrow in (c) indicates an abrupt drop in the correlation coefficient on 6–11 Apr 1993 during equatorial tides when rapid freezing and ice thickening took place.

as compared with 77% at CL and 66%–73% at OD). Equally important, the magnitude of the low-frequency variance at KM ( $844 \text{ cm}^2 \text{ s}^{-2}$ ) is approximately 2 times that at OD ( $412 \text{ cm}^2 \text{ s}^{-2}$ ) and 2.5 times that at CL ( $325 \text{ cm}^2 \text{ s}^{-2}$ ) (Table 2). Either this difference is related to significantly greater wind (or other external) forcing at station KM in comparison with the two other observational sites, or to a greater local oceanic response to this forcing. The relationship between winds and ice drift was examined using the 1993–94 OD and the 1993 KM local wind data (the CL site is not representative of oceanic winds because of the sheltering effect of nearby mountains). The fact that the wind variance in 1993 at KM ( $18.7 \text{ m}^2 \text{ s}^{-2}$ ) was consistently smaller than at OD ( $22.9 \text{ m}^2 \text{ s}^{-2}$  in 1993 and  $24.5 \text{ m}^2 \text{ s}^{-2}$  in 1994) suggests that regional differences in wind velocity cannot account for the dominance of low-frequency ice-drift variance measured at KM relative to OD.

*a. Formulation of a wind–ice drift relationship*

The simplest model describing the relationship between wind and free-ice drift in the open ocean is the Nansen–Ekman ice-drift law:

$$\mathbf{u} = \alpha_0 \exp(-i\theta_0)\mathbf{V}, \tag{6}$$

where  $\mathbf{u} = (u, v)$  is the ice-drift vector,  $\mathbf{V} = (U, V)$  is the wind vector,  $\alpha_0 \approx 0.02$  is the wind factor (a wind of  $1 \text{ m s}^{-1}$  forces a  $2 \text{ cm s}^{-1}$  ice drift), and  $\theta_0 \approx 28^\circ$  is the turning angle between the ice-drift direction and the wind direction (right of the surface wind in the Northern Hemisphere) (cf. Thorndike 1986; Wadhams 2000; Stern and Moritz 2002). Slightly different parameters in the Arctic Ocean were found by Thorndike and Colony (1982):  $\alpha_0 \sim 0.015$  and  $\theta_0 \sim 35^\circ$  in winter, and  $\alpha_0 \sim 0.018$  and  $\theta_0 \sim 42^\circ$  in summer. This seasonal change in the parameters appears mainly due to increased internal ice stresses in winter.

Another factor influencing ice-drift parameters is non-linearity. McPhee (1982, 2002) examined various non-linear sea-ice boundary layer formulations and showed that a quadratic relationship between wind and ice-drift better accounts for wind-induced motions at high wind speeds. Hibler (1986) suggests a nearly linear relation between the wind speed and ice drift for all but very low speeds, with a resulting greater sensitivity of the turning angle to the wind speed. This means that, in general, both  $\alpha_0$  and  $\theta_0$  are functions of the wind speed,  $|\mathbf{V}|$ , although in the open ocean, they are expected to be invariant to the wind direction,  $\varphi$ . The latter assumption becomes invalid near the coast. Fissel and Tang (1991) used model (6) to examine the ice-drift response to wind forcing over the northern Newfoundland shelf and found  $\alpha_0$  varies from 0.026 to 0.054 and  $\theta_0$  from  $10^\circ$  to  $63^\circ$ . Although the model was originally formulated for the open ocean, Fissel and Tang (1991) established that proximity to the coast and direction of the wind relative to the coastline are the major factors influencing variability in wind factor and turning angle. Similarly, Overland and Pease (1988) indicated a strongly anisotropic response of the ice drift to the wind near coastal boundaries.

For the region under study, the influence of the coast and direction of the local wind relative to the orientation of the coast become crucial. Model (6) does not take these effects into consideration. Therefore, to account for the low-frequency ice drift on the northwestern shelf of Sakhalin Island, we applied a two-dimensional regression model based on the regional wind. Such models are widely used in oceanography and meteorology for analysis and prediction of ocean currents and other vector processes (cf. Emery and Thomson 2001). Specifically,

$$\mathbf{u}(t) = \mathbf{A}(\tau)\mathbf{V}(t - \tau) + \mathbf{E}(t), \tag{7}$$

where

$$\mathbf{u} = \begin{pmatrix} u \\ v \end{pmatrix}, \quad \mathbf{V} = \begin{pmatrix} U \\ V \end{pmatrix}, \quad \mathbf{A} = \begin{pmatrix} a_{11} & a_{12} \\ a_{21} & a_{22} \end{pmatrix}, \quad \text{and} \tag{8}$$

$$\mathbf{E} = \begin{pmatrix} \varepsilon_u \\ \varepsilon_v \end{pmatrix};$$

$a_{ij}$  are the regression (response) coefficients linking the

TABLE 4. Regression relationships for wind and wind-induced ice drift for CRSs for 1993 and 1994.

Station, year	Cross-correlation				Regression elements				Explained variance $R^2$
	$\langle uU \rangle$	$\langle uV \rangle$	$\langle vU \rangle$	$\langle vV \rangle$	$a_{11}$	$a_{12}$	$a_{21}$	$a_{22}$	
Komvvo, 1993									
S1	0.66	-0.65	-0.60	0.68	0.90	-0.40	-3.06	2.24	0.56
S3	0.70	-0.70	-0.63	0.77	1.41	-0.57	-4.64	3.40	0.69
Odoptu, 1993									
S1	0.69	-0.57	-0.45	0.76	1.04	-0.26	-2.18	2.18	0.69
S4	0.67	-0.61	-0.35	0.78	0.95	-0.15	-2.75	2.58	0.75
Odoptu, 1994									
S1	0.80	-0.37	-0.44	0.73	1.44	-0.41	-0.73	2.51	0.58
S4	0.77	-0.36	-0.40	0.71	1.73	-0.44	-0.82	2.87	0.55

cross-shore ( $u$ ) and alongshore ( $v$ ) components of ice drift with the corresponding components ( $U$ ,  $V$ ) of wind velocity and random noise components ( $\varepsilon_u$ ,  $\varepsilon_v$ ), and  $\tau$  is the time lag between wind forcing and ice-drift response.

In the terminology of McNutt and Overland (2003), we have focused on “coherent scale” ice motions, that is, those motions having spatial scales of roughly 75–300 km and temporal scales of approximately 3–7 days. To examine the ice-drift response to the wind, we first low-pass filtered simultaneous series of wind and residual (detided) ice velocities to remove fluctuations with frequencies  $\geq 1$  cpd. The resulting low-frequency local wind and ice velocities were highly correlated. Table 4 presents mean cross-correlation and regression coefficients (averaged over the entire observational period) for CRSs Komvvo (1993) and Odoptu (1993 and 1994). Comparative results are shown for two offshore ice observation distances: 4 km (S1) for both sites, 12 km (S3) for Komvvo, and 16 km (S4) for Odoptu. The results obtained for different stations and distances are in good agreement. The best results (maximum explained variance) were obtained for zero lag ( $\tau = 0$ ), when there is no time delay between wind forcing (input) and ice-drift response (output). The explained variance for the wind-drift regression is  $R^2(\sigma_0^2 - \sigma_{\text{res}}^2)/\sigma_0^2 \approx 0.55$ – $0.75$ , where  $\sigma_0^2 = \sigma_u^2 + \sigma_v^2$  is the initial, and  $\sigma_{\text{res}}^2$  is the residual variance of the low-frequency ice drift (Table 4). Thus, 55%–75% of the total energy in low-frequency ice-drift motions is determined by the wind through the relatively simple model (7). In most cases,  $R^2$  values for the remote offshore observational areas (S3 and S4) are greater than for observational areas closest to shore (S1), where ice drift is more strongly influenced by the coast.

There are several factors that may be responsible for the unexplained variance (25%–45%) between wind and ice drift. First, this variance could, of course, be reduced by increasing the number of regression coefficients  $a_{ij}(\tau_k)$ , that is, by using more than one value for the time lag,  $\tau_k$ ,  $k = 1, 2, \dots$ . For example, Geiger et al. (1998) found 90% coherence between the modeled atmospheric field and the ice motions for the Wedell Sea.

In this case, coherence can be viewed as an estimate of the correlation integrated over a range of time lags (cf. Emery and Thomson 2001). However, it is known that multilag regression models are less stable and reliable. A second factor that may be responsible for the unexplained variances is nonlinearity (cf. McPhee 1982, 1986, 2002; Hibler 1986). To determine possible effects of nonlinear input, we undertook several calculations using wind stress (i.e., quadratic wind velocity) as the input function in (6). Surprisingly, the results were worse than with wind velocity alone ( $R^2$  was approximately 10% smaller), probably because of local characteristics of the wind and ice fields in this region. The residual variance also could be associated with time variations of the mean flow on the Sakhalin shelf (cf. Preller and Hogan 1998). Last, an important factor influencing ice drift, and probably responsible for unexplained variance, is the ice concentration and rheology (see section 5). As noted by Hibler (1986), because the force on the ice is given by the gradient of the ice stress, the ice motions may give the impression of free-ice drift in response to the winds whereas, in fact, ice stresses may be high and undergoing intense nonlinear interaction.

As was mentioned above, model (6) is described by two parameters: wind factor and turning angle, both independent on wind direction. In contrast, the four regression coefficients,  $a_{ij}$  in model (7)–(8), define the “response ellipse,” which is traced by the tip of the current velocity response vector during one complete rotation of the uniform unity wind vector (Table 4). For an isotropic (open ocean) response, the response ellipse is circular. Each response ellipse is described by four invariant parameters: the semimajor,  $A_{\text{max}}$ , and semiminor,  $A_{\text{min}}$ , ellipse axes (the maximum and minimum current responses); the orientation of the semimajor axis,  $\theta_{\text{max}}$ ; and the direction of the “effective wind” (producing maximum current response),  $\varphi_{\text{max}}$  (see the appendix for details). At this point it is worth noting the similarity between the response ellipses and ice stress or deformation ellipses (cf. Mellor 1986; Hibler 1986; Geiger et al. 1998; Richter-Menge et al. 2002). Although the processes leading to these two elliptical

structures may be related, investigation of any dynamical relationship is nontrivial and beyond the scope of the present study.

Derived response ellipses are presented in Fig. 13. As with tidal ellipses (insets in Fig. 6), all response ellipses are oriented along the coastline. The marked flatness of the response ellipses indicates that the ice reaction to the wind is strongly anisotropic: Ice response in the alongshore direction is much greater than in the cross-shore direction [ $3.0\text{--}6.0$  and  $0.2\text{--}1.5$  ( $\text{cm s}^{-1}/(\text{m s}^{-1})$ ), respectively]. The alongshore values of the response coefficients (i.e., the wind factor) are similar to those obtained by Fissel and Tang (1991) for the Newfoundland shelf [ $2.6\text{--}5.4$  ( $\text{cm s}^{-1}/(\text{m s}^{-1})$ )], but significantly greater than those estimated by Thorndike and Colony (1982) for the Arctic Ocean [ $1.5\text{--}1.8$  ( $\text{cm s}^{-1}/(\text{m s}^{-1})$ )]. Response ellipses for the remote offshore observational areas (S3, S4) are from 50% (KM) to 15%–20% (OD) greater than for the areas closest to shore (S1). As in the Nansen–Ekman theory, ice-drift vectors are mainly directed to the right of the wind direction. Thus, even winds blowing cross-shore can generate alongshore ice drift. Vectors of maximum ice drift are typically directed  $20^\circ\text{--}40^\circ$  clockwise to the “effective wind” direction, close to the theoretical Nansen–Ekman angle of  $28^\circ$  for the open ocean and findings by Thorndike and Colony (1982), Fissel and Tang (1991), and Stern and Moritz (2002). However, in contrast to the Nansen–Ekman theory, turning angles of the ice drift and the wind vectors are highly nonuniform. In particular, for closely meridional winds, ice motions are directed counterclockwise to the wind vector (Fig. 13).

The response ellipses for radar sites KM and OD for 1993 are quite similar; in both cases, the ellipses are almost flat and have similar angles of the ice drift relative to the wind vectors (pairs of thick and thin arrows isolated in the four quadrants of Fig. 13). However, the KM ellipse is about 1.5 times as long, suggesting that wind-induced alongshore ice drift in the vicinity of site KM is 1.5 times that in the vicinity of site OD. This explains why the variance of low-frequency ice-drift motions at KM is more than 2 times that at OD (Table 2). This difference may be related to the relatively gently deepening continental shelf and slope seaward of site KM (line 13 in Fig. 9c). The relatively shallow depths in this region appear to support the formation of intense, wind-induced, low-frequency currents. We assume that wind-induced currents are stronger in this region because momentum transferred from the wind to the currents is distributed over a thinner portion of the water column.

Although model (7)–(8) is clearly an oversimplification, it is consistent with our attempt to characterize the dominant low-frequency mechanisms forcing spatial and temporal variability in ice drift on the Sakhalin shelf. In general, higher-order models are likely needed, especially for regions undergoing marked deformation and shear. McPhee (1986, 2002) and Hibler (1986) also

emphasize the considerable effects attributed to ice–water boundary layers, ice rheology, and other dynamical factors.

#### b. Time variation of ice drift

The main features of the ice-drift response ellipses (orientation, shape, and turning angles) at two different sites (KM and OD) computed for the same year (1993) are similar (Fig. 13). In contrast, the response ellipses at the same site (OD) but for two different years (1993 and 1994) are significantly different. The 1994 ellipses for both the nearshore (S1) and offshore (S4) distances are more circular, suggesting a stronger cross-shore wind response when compared with 1993. Also, turning angles between the direction of the wind and ice drift in 1994 were smaller when compared with those for 1993. We assume that these differences arise from the higher ice concentration in 1993 when compared with 1994.

To estimate the influence of ice concentration on wind-induced ice drift, we divided the 1993 data into four 20-day segments and examined these segments separately. The four time segments were characterized by markedly different ice type and concentration (Tambovsky et al. 2001): 1) the first period (centered on 21 March) had an ice concentration of approximately 80%–90% with the ice field consisting of large and small broken floes; 2) the second period (centered on 9 April) had the highest ice concentration (95%–100%), consisting of large ice fields; 3) the third period (centered on 27 April) consisted of gradually melting ice, with reduced concentration (60%–80%) and diminished flow sizes; and 4) the last period (centered on 13 May) was associated with intensive ice melting, during which time the ice concentration reduced to 40%–50% and the ice mostly had the character of shuga. The computed response ellipses (Fig. 14) demonstrate significant temporal changes in the ice-drift response to the wind, apparently reflecting the corresponding changes in ice features. During the period of the highest ice concentration (the second period), the response ellipses became almost flat, indicating that the ice-drift response was almost rectilinear (alongshore). Even the magnitude of the alongshore response (major ellipse axis) was smaller during this period in comparison with the others. During the early spring (the first period), and especially during the third period, the response ellipses became larger and more circular, indicating the presence of more intensified cross-shore ice motions. Last, during the late spring (the fourth period) the response ellipses changed from flat to oval. Apparently, the last period corresponds to a time of free-ice drift, while other periods reflect a strong interaction between the internal ice stress and the coast. This effect was maximum during the second period. These results are in good agreement with theoretical studies on the influence of ice stress on ice motions and are consistent with Hibler (1986): “The most ob-

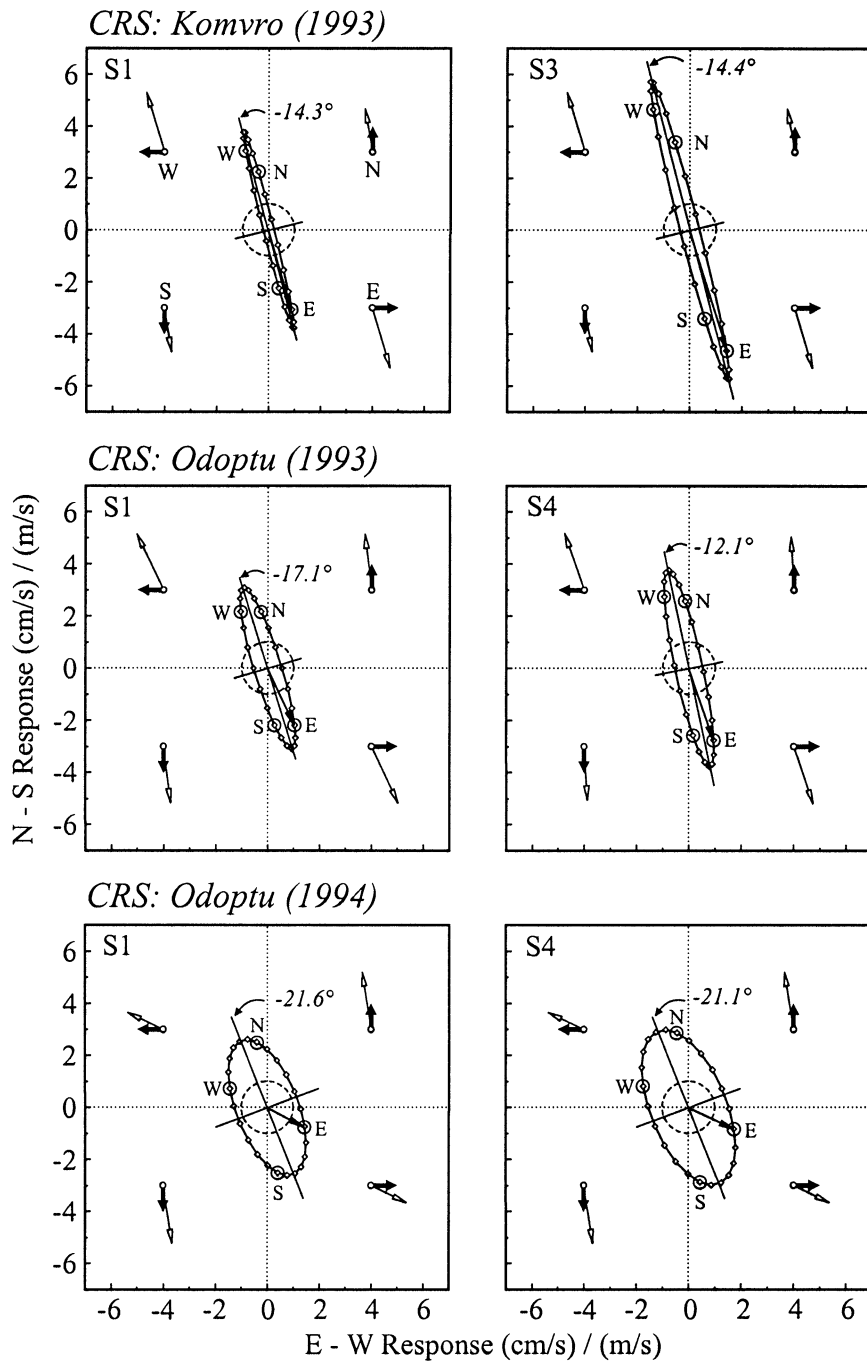


FIG. 13. Response ellipses for CRSs KM (1993) and OD (1993 and 1994). Ellipse orientations are in degrees counterclockwise from north (up) in each panel. The small dashed circles represent a uniform isotropic 0.01 ice-drift response (of  $1 \text{ cm s}^{-1}$  due to a wind of  $1 \text{ m s}^{-1}$ ). Letters "W," "N," "E," and "S" give the observed speed and direction of the ice drift in response to winds blowing toward the west, north, east, and south, respectively. Also shown are the directions of ice drift (thin arrows) for each of the four main compass wind directions (thick solid arrows), beginning with westward winds in the top-left panel. (left) The 4-km offshore distance (S1); (right) the 12- (S3) and 16-km (S4) offshore distance.

CRS: Odoptu (1993)

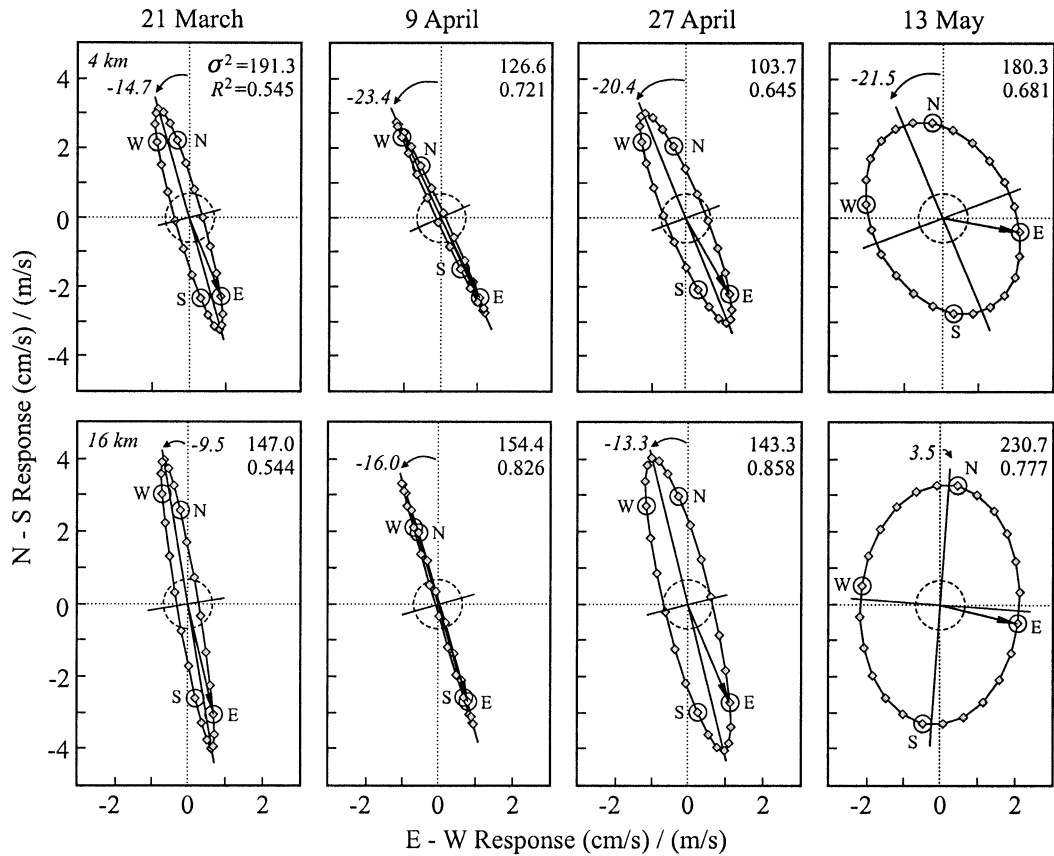


FIG. 14. Time variations of response ellipses for CRS OD (1993) at two offshore observation sites: (top) 4 and (bottom) 16 km. Ellipse calculations are made for 20-day periods centered at the day indicated at the top of each panel. (See caption to Fig. 13 for further details.) The ice-drift variance ( $\sigma^2$ ) and explained variance ( $R^2$ ) are indicated for each ellipse.

vious effect of the ice stress is to change the ice drift direction and magnitude from the free drift case.”

To examine variations over time in the low-frequency winds and associated ice-drift motions, we used a multiple filter technique (MFT) similar to wavelet analysis (cf. Emery and Thomson 2001; Rabinovich and Thomson 2001). For this analysis, we selected simultaneous low-frequency series of wind and offshore (16 km) ice drift at CRS OD from 12 March to 22 May 1993 and focused on the frequency band from 0.03 to 0.6 cpd (periods from approximately 33 to 1.7 days). The  $f-t$  diagrams (Fig. 15b) reveal a very close similarity between time variations in the alongshore wind ( $V$ ) and alongshore ice drift ( $v$ ). Close agreement of these motions is observed in both frequency and time, with the main energy bands centered at periods of 10–11, 5, and 2.5 days. It is evident from these plots that time-frequency variations in the alongshore wind are the primary cause of the ice-drift velocity fluctuations.

Variations in the cross-shore component of the wind and coincident ice motions were poorly correlated for about two-thirds of the observational period. The situ-

ation changed dramatically after yearday 120 (30 April 1993) when variations in the wind velocity and ice drift became similar in both the frequency and time domains (Fig. 15a). A possible cause for this change is that, by the end of April, the ice cover had begun to break into smaller ice floes and to melt, creating larger areas of open water, allowing the ice pack to more easily respond to the cross-shore wind component. These results are consistent with the results from the response ellipses shown in Fig. 14. Thus, during high ice concentrations (when the sea ice is most extensive and internally cohesive), the ice drift is almost entirely alongshore and highly correlated with the respective component of the wind stress. However, in late spring, when sea ice becomes broken and patchy (i.e., free), it responds to both the cross-shore and alongshore components of the wind.

5. Discussion and conclusions

High-quality radar ice-velocity measurements for the northeastern shelf of Sakhalin Island, combined with

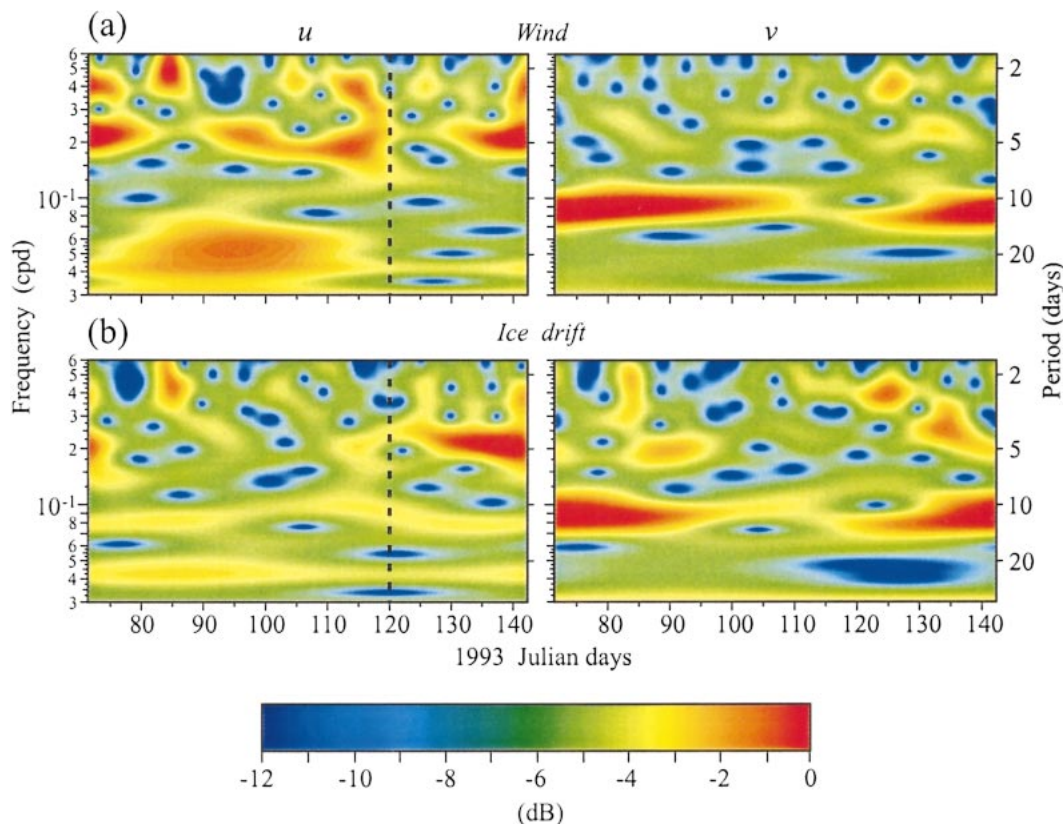


FIG. 15. Multiple filter analysis (MFA) of (left) cross-shore and (right) alongshore velocity components of (a) wind and (b) ice drift as functions of frequency and time for CRS OD for 1993. The legend shows amplitude isolines (dB) relative to the maximum amplitudes of  $6.4 \text{ m s}^{-1}$  for (a) and  $24 \text{ cm s}^{-1}$  for (b). Dashed vertical line in (a) and (b) indicates the beginning of the free-ice period when there was high correlation between the cross-shore components of wind and ice drift.

current-meter and coastal wind data, provide reasonable spatial and temporal delineation of sea-ice motions in this region of active oil and gas exploration. Findings reveal that ice drift on the Sakhalin shelf is associated with two major mechanisms: diurnal tidal currents and wind-induced surface drift, which together account for 92%–95% of the total variance in the ice-drift records. On the northern part of the shelf, diurnal tidal motions alone account for about 70%–80% of the drift variance. Combined tidal and wind-induced ice-drift motions in this region again reach maximum velocities of about  $1.5 \text{ m s}^{-1}$ . In contrast, over the central part of the shelf ( $\sim 51.2^\circ\text{N}$ ), tidal motions account for only 3% of the drift variance, with about 90% due to wind-induced low-frequency currents.

During 1994, maximum observed alongshore tidal ice-drift velocities were  $\sim 90$ – $110 \text{ cm s}^{-1}$  at CL,  $70$ – $100 \text{ cm s}^{-1}$  at OD, and  $10$ – $15 \text{ cm s}^{-1}$  at KM. The high speeds of the tidal ice drift for CL and OD are associated with strong  $K_1$  and  $O_1$  tidal currents. Taking into account the 18.6-yr nodal cycle, we expect that in 2006–07 (the next period of extreme diurnal tides) the tidal currents will be about 25% stronger and likely to reach  $120$ –

$140 \text{ cm s}^{-1}$ . These strong motions could play a major role in the regional ice rheology and response.

Our analyses are the first to show that alongshore variations in tidal ice-drift velocity off the northeastern coast of Sakhalin Island is mainly due to topographically induced changes in diurnal shelf waves. In particular, the relatively steep continental margin north of  $52.0^\circ\text{N}$  is highly conducive to the generation diurnal barotropic shelf waves and associated strong tidal currents and less conducive to the formation of wind-induced currents. In contrast, the relatively gently sloping continental margin seaward of site KM ( $\sim 51.2^\circ\text{N}$ ) cannot support diurnal shelf waves (the primary cause for strong diurnal tidal currents and ice drift throughout the rest of this region) but is amenable to the formation of intense wind-induced currents and related ice drift.

The tidal ice-drift ellipses for diurnal motions on the northeastern Sakhalin shelf are in agreement with the corresponding ellipses obtained from current-meter observations and correspond closely with results of barotropic numerical modeling by Kowalik and Polyakov (1998). The close agreement between radar-measured ice drift, moored current-meter observations for differ-

ent years and seasons, and numerical modeling indicates that the tidal motions in this region are mainly barotropic. Results further suggest that the diurnal tidal waves propagate southward along the northeastern coast of Sakhalin forming three distinct zones: 1) a zone of large-amplitude diurnal tidal currents bordering the northeastern end of Sakhalin Island, 2) a zone of rapidly diminishing diurnal tidal velocities beginning around 51.5°N latitude, and 3) a zone of minimum currents at approximately 51.0°–51.2°N latitude (in the vicinity of site KM).

Because tidal forcing is almost totally deterministic, the previous findings suggest that measurements of tidal currents can serve as ice-drift proxy data for use in numerical and analytical models to forecast free tidal ice drift. However, the “free-ice approximation” for overall ice-drift description in this region is invalid during high ice concentration. For example, the 1994 ice concentration on the northeastern shelf of Sakhalin Island was low (50%–70%), while the year 1993 had the most extensive ice cover (80%–90%) (Preller and Hogan 1998). Consequently, diurnal ice-drift velocities observed during the low ice concentration year 1994 were similar to summer tidal velocities recorded in other years (1980–98). In contrast, the ice-drift velocities recorded during in the high ice concentration year 1993 were approximately 25%–30% weaker than in 1994.

In addition to the effects of ice concentration, the interaction of tidal currents and ice on the northeastern shelf of Sakhalin Island involves complicated feedback processes. For example, the area of broken ice in the satellite image in Fig. 2 closely coincides with the zone of strong diurnal tidal currents (Fig. 6) located on the Sakhalin shelf north of 52°N. The fact that the Sakhalin polynya is commonly observed in this zone (Wakatsuchi and Martin 1990; Martin et al. 1998) indicates that the intensive tidal currents in this region contribute to ice breaking and the maintenance of open water. Thus, the free-ice approximation is more applicable to regions having strong diurnal currents than regions with weak to moderate diurnal currents.

Our analysis suggests that low-frequency ice-drift oscillations on the Sakhalin shelf are mainly wind generated and that there is no detectable time shift between the wind and wind-induced ice drift. A vector regression model enables us to explain 55%–75% of the total energy in the low-frequency ice-drift motions. The response ellipses derived from the model determine the wind-forced velocity of the ice drift as a function of the wind direction. The marked flatness of these ellipses indicates that the ice-drift velocity in response to the wind is highly anisotropic, with the alongshore response of the ice-drift considerably greater than the cross-shore response. For a known wind velocity, the response ellipses enable us to predict the associated ice drift. The problem here, however, is similar to that for tidal drift in that internal ice stresses appear to significantly affect the ice-drift response to the wind, with the stress-in-

duced changes in regression ellipses even stronger than for tidal ellipses. Specifically, when ice concentration is high, ellipses become almost flat (indicating the predominance of rectilinear alongshore wind-generated ice motions), while for free ice they are more circular, indicating a much greater contribution from the cross-shore component of ice motion (i.e., more like open ocean conditions). Accurate information on ice concentration is crucial for the correct prediction of wind-induced ice drift.

We acknowledge that the computation and prediction of ice motions are not sufficient to describe and predict the complex deformation structures, shear zones, and other ice properties. Simple linear regressive models can provide only rough indications of the internal ice stress and strain-rate relationships. High-quality sea-ice boundary layer data along with comprehensive nonlinear numerical models are needed to correctly simulate these ice features (cf. Hibler 1986; McPhee 1982, 1986, 2002; Geiger et al. 1998; Heil and Hibler 2002). Nevertheless, information such as we have provided on the strength and variability of ice motions enable us to construct these models more efficiently.

Comparison of the 1993 and 1994 results, as well as other information on ice in the Sea of Okhotsk (cf. Wakatsuchi and Martin 1990; Martin et al. 1998; Preller and Hogan 1998; Tambovsky et al. 2001), demonstrates significant month-to-month and year-to-year variations in ice coverage and compactness. As in the case for the beginning of April 1993, high ice concentrations can lead to substantial reduction of tidal ice drift, as well as the reduced ice-drift response to the wind. These, in turn, can significantly affect operations on drill platforms. Although it would appear that free-moving fast-moving floes observed in late spring (which can have speeds exceeding  $1.8 \text{ m s}^{-1}$ ) pose the greatest danger for these platforms, changes in tidal current and wind response associated with changes in ice concentration are still of prime importance to drill platforms and detract from our ability to predict sea-ice drift on the Sakhalin Island shelf. The mechanics, anisotropic distortion of the ice field, and resulting stress fields will have a detrimental impact on offshore platforms and other marine structures. The effects of ice deformation, in which ice moves cohesively, will compound motions associated with ice drift.

*Acknowledgments.* We thank Zygmunt Kowalik, University of Alaska, Fairbanks, who kindly supplied us with the results of numerical computation of tidal currents for the shelf of Sakhalin Island. Isaac Fine, Institute of Heat and Mass Transfer, Minsk, Belarus, provided us with numerical computations of shelf waves, and Patricia Kimber helped to draft the figures. We also thank the two anonymous referees for very helpful and informative comments.

## APPENDIX

## Regression Coefficients and Response Ellipse Parameters

To determine the regression coefficients  $a_{ij}$  in (7), we apply a least squares method and obtain the matrix relation

$$\mathbf{AD} = \mathbf{R}, \quad (\text{A1})$$

where  $\mathbf{A}$  is the matrix of regression coefficients  $a_{ij}$  determined by expression (8),  $\mathbf{R}$  is the cross-correlation matrix of input versus output correlation coefficients, and  $\mathbf{D}$  is the autocorrelation matrix of the input function (wind):

$$\mathbf{R} = \begin{pmatrix} r_{uU}^2 & r_{uV}^2 \\ r_{vU}^2 & r_{vV}^2 \end{pmatrix} = \begin{pmatrix} \langle uU \rangle & \langle uV \rangle \\ \langle vU \rangle & \langle vV \rangle \end{pmatrix} \quad \text{and}$$

$$\mathbf{D} = \begin{pmatrix} r_{UU}^2 & r_{UV}^2 \\ r_{UV}^2 & r_{VV}^2 \end{pmatrix} = \begin{pmatrix} \langle UU \rangle & \langle UV \rangle \\ \langle UV \rangle & \langle VV \rangle \end{pmatrix}, \quad (\text{A2})$$

where  $\langle \rangle$  denotes time averages. From (A1), it follows that

$$\mathbf{A} = \mathbf{RD}^{-1}, \quad (\text{A3})$$

where  $\mathbf{D}^{-1}$  is the inverse of  $\mathbf{D}$ . Equation (A3) specifies the four regression (response) coefficients:  $a_{11}$ ,  $a_{12}$ ,  $a_{21}$ , and  $a_{22}$ . Four parameters of the “response ellipse” may be found from these coefficients:

- 1) *Direction of “effective (noneffective) wind”*:  $\varphi_{\max}$  ( $\varphi_{\min}$ ), that is, the wind direction producing the maximum (minimum) current response:

$$\varphi_{\max} (\varphi_{\min}) = \frac{1}{2} \arctan \left[ \frac{2(a_{11}a_{12} + a_{21}a_{22})}{(-a_{11}^2 + a_{12}^2 - a_{21}^2 + a_{22}^2)} \right], \quad (\text{A4})$$

where  $\varphi_{\max}$  ( $\varphi_{\min}$ ) is measured clockwise from north. Directions of the maximum  $\varphi_{\max}$  and minimum  $\varphi_{\min}$  responses are related to one other by  $\varphi_{\min} = \varphi_{\max} \pm 90^\circ$ .

- 2) *Semimajor ellipse axes*:

$$A_{\max} = [(a_{11} \sin \varphi_{\max} + a_{12} \cos \varphi_{\max})^2 + (a_{21} \sin \varphi_{\max} + a_{22} \cos \varphi_{\max})^2]^{1/2}. \quad (\text{A5})$$

- 3) *Seminor ellipse axes*:

$$A_{\min} = [(a_{11} \sin \varphi_{\min} + a_{12} \cos \varphi_{\min})^2 + (a_{21} \sin \varphi_{\min} + a_{22} \cos \varphi_{\min})^2]^{1/2}. \quad (\text{A6})$$

- 4) *Orientation of the semimajor axis*:

$$\theta_{\max} = \arctan \left( \frac{a_{11} \sin \varphi_{\max} + a_{12} \cos \varphi_{\max}}{a_{21} \sin \varphi_{\max} + a_{22} \cos \varphi_{\max}} \right). \quad (\text{A7})$$

## REFERENCES

- Alfulit, M. A., and S. Martin, 1987: Satellite passive microwave studies of the Sea of Okhotsk ice cover and its relation to oceanic processes, 1978–1982. *J. Geophys. Res.*, **92** (C12), 13 013–13 028.
- Brink, K. H., and D. C. Chapman, 1987: Programs for computing properties of coastal-trapped waves and wind-driven motions over the continental shelf and slope. 2d ed. Woods Hole Oceanographic Institution Tech. Rep. WHOI-87-24, 119 pp.
- Crawford, W. R., and R. E. Thomson, 1984: Diurnal-period continental shelf waves along Vancouver Island: A comparison of observations with theoretical models. *J. Phys. Oceanogr.*, **14**, 1629–1646.
- Emery, W. J., and R. E. Thomson, 2001: *Data Analysis Methods in Physical Oceanography*. 2d ed. Elsevier, 638 pp.
- Fissel, D. B., and C. L. Tang, 1991: Response of sea ice drift to wind forcing on the northeastern Newfoundland shelf. *J. Geophys. Res.*, **96** (C10), 18 397–18 409.
- Foreman, M. G. G., and R. E. Thomson, 1997: Three-dimensional model simulations of tides and buoyancy currents along the west coast of Vancouver Island. *J. Phys. Oceanogr.*, **27**, 1300–1325.
- Geiger, C. A., W. D. Hibler III, and S. F. Ackley, 1998: Large-scale ice drift and deformation: Comparison between models and observations in the western Weddell Sea during 1992. *J. Geophys. Res.*, **103** (C10), 21 893–21 913.
- Heil, P., and W. D. Hibler, 2002: Modeling the high-frequency component of Arctic sea ice drift and deformation. *J. Phys. Oceanogr.*, **32**, 3039–3057.
- Hibler, W. D., III, 1986: Ice dynamics. *The Geophysics of Sea Ice*, N. Untersteiner, Ed., Plenum, 577–640.
- Kowalik, Z., and I. Polyakov, 1998: Tides in the Sea of Okhotsk. *J. Phys. Oceanogr.*, **28**, 1389–1409.
- LeBlond, P. H., and L. A. Mysak, 1978: *Waves in the Ocean*. Elsevier, 602 pp.
- Martin, S., R. Drucker, and K. Yamashita, 1998: The production of ice and dense shelf water in the Okhotsk Sea polynyas. *J. Geophys. Res.*, **103** (C12), 27 771–27 782.
- McNutt, S. L., and J. E. Overland, 2003: Spatial hierarchy in Arctic sea ice dynamics. *Tellus*, **55A**, 181–191.
- McPhee, M. G., 1982: Sea ice drag laws and simple boundary layer concepts, including application to rapid melting. U.S. Army Cold Regions Research and Engineering Laboratory Rep. 82-4, 25 pp.
- , 1986: The upper ocean. *The Geophysics of Sea Ice*, N. Untersteiner, Ed., Plenum, 339–394.
- , 2002: Turbulent stress at the ice/ocean interface and bottom surface hydraulic roughness during the SHEBA drift. *J. Geophys. Res.*, **107** (C10), 8037, doi:10.1029/2000JC000633.
- Mellor, M., 1986: Mechanical behavior of sea ice. *The Geophysics of Sea Ice*, N. Untersteiner, Ed., Plenum, 165–281.
- Mysak, L. A., 1980: Recent advances in shelf wave dynamics. *Rev. Geophys. Space Phys.*, **18**, 211–241.
- Nakamura, T., T. Awaji, T. Hatayama, and K. Akitomo, 2000: Tidal exchange through the Kuril Straits. *J. Phys. Oceanogr.*, **30**, 1622–1644.
- Ohshima, K. I., M. Wakatsuchi, Y. Fukamachi, and G. Mizuta, 2002: Near-surface circulation and tidal currents of the Okhotsk Sea observed with satellite-tracked drifters. *J. Geophys. Res.*, **107**, 3195, doi:10.1029/2001JC001005.
- Overland, J. E., and C. H. Pease, 1988: Modeling ice dynamics of coastal seas. *J. Geophys. Res.*, **93** (C12), 15 619–15 637.
- Padman, L., and C. Kottmeier, 2000: High-frequency ice motion and divergence in the Weddell Sea. *J. Geophys. Res.*, **105** (C2), 3379–3400.
- , A. D. Plueddemann, R. D. Muench, and R. Pinkel, 1992: Diurnal tides near the Yermak Plateau. *J. Geophys. Res.*, **97**, 12 639–12 652.
- Pokrasenko, S. A., P. A. Truskov, and L. P. Yakunin, 1987: Investigation of sea-ice drift on the shelf of Sakhalin Island using the radar methods (in Russian). *Proc. Tr. Far East. Res. Inst. DVNII*, **36**, 49–52.

- Popudribko, K. K., V. F. Putov, and G. V. Shevchenko, 1998: Estimation of characteristics of sea currents in the Piltun-Astokh oil and gas-bearing area (northeastern Sakhalin shelf). *Russ. Meteor. Hydrol.*, **4**, 60–71.
- Preller, R. H., and P. J. Hogan, 1998: Oceanography of the Sea of Okhotsk and the Japan/East Sea. *The Sea*, A. R. Robinson and K. H. Brink, Eds., The Global Coastal Ocean, Vol. 11, John Wiley and Sons, 429–481.
- Pugh, D. T., 1987: *Tides, Surges and Mean Sea-Level*. John Wiley and Sons, 472 pp.
- Putov, V. F., and G. V. Shevchenko, 1998: Peculiar tidal regime of north-eastern Sakhalin shelf: Specific features of tidal regime on the northeastern shelf of Sakhalin Island (in Russian). *FERHRI Proc. Hydrometeorological Processes on the Shelf: Impact Assessment on the Water*, Vladivostok, Russia, DVO RAN, 61–82.
- Rabinovich, A. B., and G. V. Shevchenko, 1984: Two-step mechanism for dissipation of tidal energy in the ocean. *Trans. Dokl. USSR Acad. Sci., Earth Sci. Sect.*, **276**, 228–231.
- , and A. E. Zhukov, 1984: Tidal oscillations on the shelf of Sakhalin Island. *Oceanology*, **24**, 184–189.
- , and R. E. Thomson, 2001: Evidence of diurnal shelf waves in satellite-tracked drifter trajectories off the Kuril Islands. *J. Phys. Oceanogr.*, **31**, 2650–2668.
- Richter-Menge, J. A., S. L. McNutt, J. E. Overland, and R. Kwok, 2002: Relating arctic pack ice stress and deformation under winter conditions. *J. Geophys. Res.*, **107**, 8040, doi:10.1029/2000JC000477.
- Stern, H. L., and R. E. Moritz, 2002: Sea ice kinematics and surface properties from RADARSAT synthetic aperture radar during the SHEBA drift. *J. Geophys. Res.*, **107**, 8028, doi:10.1029/2000JC000472.
- Suzuki, K., and S. Kanari, 1986: Tidal simulation of the Sea of Okhotsk (in Japanese with English abstract). *Kaiyo Kagaku*, **18**, 455–463.
- Tambovsky, V. S., E. A. Tikhonchuk, and G. V. Shevchenko, 2001: Characteristics of morphometry and dynamics of sea ice on the northeastern shelf of Sakhalin Island. *Proc. 16th Int. Symp. on Okhotsk Sea and Sea Ice*, Mombetsu, Hokkaido, Japan, The Okhotsk Sea and Cold Ocean Research Association, 356–390.
- Thorndike, A. S., 1986: Kinematics of the sea ice. *The Geophysics of Sea Ice*, N. Untersteiner, Ed., Plenum, 489–549.
- , and R. Colony, 1982: Sea ice motion response to geostrophic winds. *J. Geophys. Res.*, **87** (C8), 5845–5852.
- Wadhams, P., 2000: *Ice in the Ocean*. Gordon and Breach, 351 pp.
- Wakatsuchi, M., and S. Martin, 1990: Satellite observations of the ice cover of the Kuril Basin region of the Okhotsk Sea and its relation to the regional oceanography. *J. Geophys. Res.*, **95** (C8), 13 393–13 410.
- , and K. I. Ohshima, 1990: Observations of ice-ocean eddy streets in the Sea of Okhotsk off the Hokkaido coast using radar images. *J. Phys. Oceanogr.*, **20**, 585–594.
- Yefimov, V. V., and A. B. Rabinovich, 1980: Resonant tidal currents and their relation to continental shelf waves of the northwestern Pacific Ocean. *Izv. Atmos. Oceanic Phys.*, **16**, 805–812.